European Journal of Medicinal Chemistry 220 (2021) 113470

Contents lists available at ScienceDirect

European Journal of Medicinal Chemistry

journal homepage: http://www.elsevier.com/locate/ejmech

Synthesis, biological, and photophysical studies of molecular rotor-based fluorescent inhibitors of the trypanosome alternative oxidase

Eduardo J. Cueto-Díaz [a, 1], Godwin U. Ebiloma [b, c, d], Ibrahim A. Alfayez [c], Marzuq A. Ungogo [c, e], Leandro Lemgruber [c], M. Carmen González-García [f], Maria D. Giron [g], Rafael Salto [g], Francisco José Fueyo-González [a], Tomoo Shiba [b], Juan A. González-Vera [f], Maria José Ruedas Rama [f], Angel Orte [f], Harry P. de Koning [c], Christophe Dardonville [a, *]

[a] Instituto de Química Médica, IQM–CSIC, Juan de la Cierva 3, E–28006, Madrid, Spain
[b] Graduate School of Science and Technology, Department of Applied Biology, Kyoto Institute of Technology, Kyoto, 606-8585, Japan
[c] Institute of Infection, Immunity and Inflammation, College of Medical, Veterinary and Life Sciences, University of Glasgow, Glasgow, United Kingdom
[d] School of Health and Life Sciences, Teesside University, Middlesbrough, United Kingdom
[e] Department of Veterinary Pharmacology and Toxicology, Faculty of Veterinary Medicine, Ahmadu Bello University, Zaria, Nigeria
[f] Departamento de Fisicoquimica, Facultad de Farmacia, Universidad de Granada, C. U. Cartuja, E–18071, Granada, Spain
[g] Departamento de Bioquimica y Biologia Molecular II. Facultad de Farmacia, Universidad de Granada, C. U. Cartuja, E–18071, Granada, Spain

ARTICLE INFO

Article history:
Received 1 February 2021
Received in revised form
26 March 2021
Accepted 10 April 2021
Available online 16 April 2021

Keywords:
Trypanosome alternative oxidase (TAO) inhibitor
Trypanosoma brucei
Molecular rotor
Fluorescent probe
2,4-dihydroxybenzoic acid derivative
Julolidine

ABSTRACT

We have recently reported on the development and trypanocidal activity of a class of inhibitors of Trypanosome Alternative Oxidase (TAO) that are targeted to the mitochondrial matrix by coupling to lipophilic cations via C14 linkers to enable optimal interaction with the enzyme's active site. This strategy resulted in a much-enhanced anti-parasite effect, which we ascribed to the greater accumulation of the compound at the location of the target protein, i.e. the mitochondrion, but to date this localization has not been formally established. We therefore synthesized a series of fluorescent analogues to visualize accumulation and distribution within the cell. The fluorophore chosen, julolidine, has the remarkable extra feature of being able to function as a viscosity sensor and might thus additionally act as a probe of the cellular glycerol that is expected to be produced when TAO is inhibited. Two series of fluorescent inhibitor conjugates incorporating a cationic julolidine-based viscosity sensor were synthesized and their photophysical and biological properties were studied. These probes display a red emission, with a high signal-to-noise ratio (SNR), using both single- and two-photon excitation. Upon incubation with *T. brucei* and mammalian cells, the fluorescent inhibitors **1a** and **2a** were taken up selectively in the mitochondria as shown by live-cell imaging. Efficient partition of **1a** in functional isolated (rat liver) mitochondria was estimated to 66 ± 20% of the total. The compounds inhibited recombinant TAO enzyme in the submicromolar (**1a**, **2c**, **2d**) to low nanomolar range (**2a**) and were effective against WT and multidrug-resistant trypanosome strains (B48, AQP1-3 KO) in the submicromolar range. Good selectivity (SI > 29) over mammalian HEK cells was observed. However, no viscosity-related shift could be detected, presumably because the glycerol was produced cytosolically, and released through aquaglyceroporins, whereas the probe was located, virtually exclusively, in the trypanosome's mitochondrion.
© 2021 The Author(s). Published by Elsevier Masson SAS. This is an open access article under the CC BY-NC-ND license (http://creativecommons.org/licenses/by-nc-nd/4.0/).

1. Introduction

Sleeping sickness, a parasitic disease caused by African trypanosomes (i.e. *T. brucei gambiense* and *T. b. rhodesiense*), is a neglected tropical disease that put millions of people at risk in sub-Saharan Africa [1]. The parasites are transmitted by the bite of infected tsetse flies and the illness takes place in two phases: an

* Corresponding author.
E-mail address: dardonville@iqm.csic.es (C. Dardonville).
[1] Current affiliation: Centro de Astrobiología, CSIC–INTA, E–28850 Torrejón de Ardoz, Spain.

https://doi.org/10.1016/j.ejmech.2021.113470
0223-5234/© 2021 The Author(s). Published by Elsevier Masson SAS. This is an open access article under the CC BY-NC-ND license (http://creativecommons.org/licenses/by-nc-nd/4.0/).

early hemolymphatic stage with few specific symptoms that is followed by a central nervous system infection leading to the death of the patient. Treatment options for sleeping sickness have relied for decades on relatively toxic drugs that require long administration protocols and hospitalization of the patients [2]. In the last years, a new orally active drug, fexinidazole, has been registered for both stages of *gambiense* sleeping sickness. Even though the approval of fexinidazole constitutes important progress in the battle against the disease, the possible occurrence of cross-resistance between the two nitroimidazole drugs fexinidazole and nifurtimox (both used for late-stage *gambiense* HAT) should not be overlooked. Moreover, *rhodesiense* sleeping sickness is still the most neglected disease with only suramin (early stage) and the extremely toxic arsenical melarsoprol in propylene glycol for the late-stage disease [2]. Moreover, *brucei*-group trypanosomes including *T. b. brucei, T. vivax, T. congolense, T. evansi* and *T. equiperdum* are involved in diseases of valuable livestock, not just in Africa but also in South America and Asia [3]. Hence, the search for new compounds with different modes of action against *T. brucei* and related species remains an important goal in tropical diseases research.

Bloodstream form (BSF) trypomastigotes, the human-infective form of *T. brucei*, depend on aerobic glycolysis for their energy supply because they have no functional oxidative phosphorylation pathway [4]. In its place, they use a plant-like alternative oxidase (trypanosome alternative oxidase, TAO) to re-oxidize the NADPH that is produced during glycolysis [5]. This enzyme, which is an interfacial inner mitochondrial membrane protein [6,7], is unique and essential to BSF trypanosomes; inhibitors of TAO have shown in vitro and *in vivo* activity in mouse models of trypanosomiasis, showing the potential of this target for chemotherapy [8].

In earlier studies, we showed that it was possible to enhance the trypanocidal activity of TAO inhibitors using lipophilic cations (LC; triphenylphosphonium or quinolinium salts), which are used as mitochondrion-targeting moieties (Chart 1). The inhibitor and LC group must be separated by a long flexible chain, typically consisting of 14 methylene units, to allow optimal interaction with the TAO catalytic site [8–11]. However, to date we have not been able to verify the extent to which these LC-coupled inhibitors, featuring the unusual long linkers, do distribute to the trypanosome mitochondrion, nor the dynamics of the cellular uptake of the drugs by the parasites.

Here, we report the synthesis, photophysical characterization, and biological activity of fluorescent TAO inhibitor probes (**1a**, **2a**–**d**) that incorporate a julolidine-based molecular rotor with a cationic pyridinium salt as mitochondrial targeting moiety (Fig. 1). (E)-4-(2-(8-hydroxy-julolidine-9-yl)vinyl-1-methylpyridine-1-ium bromide (HJVPI) was chosen for its compact and lipophilic nature, which would not meaningfully interfere with cellular distribution engendered by the LC group, and its low cytotoxicity, as well as for its photophysical properties (red emitting fluorescence) [12]. Moreover, as a molecular rotor, this group can function as a viscosity sensor, which might allow the detection of the cellular glycerol produced as a metabolic consequence of TAO inhibition, thereby reporting on both the localization and the effectiveness of the probe as an on-target inhibitor.

Molecular rotors are fluorescent probes known to form twisted intramolecular charge-transfer (TICT) complexes in the excited state, the fluorescence quantum yield of which is dependent on the nearby milieu [13]. The new probes **1a** and **2a**–**d** generated a red, high signal-to-noise ratio (SNR) emission and single-/two-photon excitation fluorescence that allowed precise mitochondrial localization in trypanosomes and human cells. The rotational properties make these TAO inhibitors sensitive to viscosity changes (i.e. inside the mitochondrion or in the presence of glycerol): a weak emission was observed in non-viscous media whereas a higher fluorescence was observed in high viscosity medium due to the restriction of the free rotation of the molecular rotor [14]. As the inhibition of TAO leads to a shift in trypanosomal glucose metabolism and the production of large amounts of glycerol as a glycolytic end product [8,15], we investigated the possibility that these molecular probes would allow not only the study of the uptake and distribution of LC-coupled TAO inhibitors in trypanosomes, but also the real-time monitoring of TAO inhibition itself, through the production of cellular glycerol.

2. Results and discussion

2.1. Synthesis of compounds 1a, 2a–d, and 12

Compound **1a** was prepared in five synthetic steps from commercially available orcinol **3** (Scheme 1). Formylation of **3** under Vilsmeier-Haack conditions led to **4** in good yields (73%); subsequent Pinnick oxidation yielded **5a**. In the next step, selective chlorination of **5a** was problematic as a mixture of mono- (**5c**, ~30%) and di-chlorinated (**5b**, ~70%) compounds was obtained. Isolation of pure **5c** was not achieved as both **5b** and **5c** displayed similar R_fs. Different protocols were tried (e.g. working at −20 °C, modifying reaction time or equiv. of reagents, etc.) to obtain the pure mono-chlorinated compound **5c** following this strategy [16,17]. However, we were unable to reproduce the reported results (i.e. 92% yield of the monochlorinated compound **5b** after column chromatography) [17] after several attempts. However, when freshly purchased acetaldehyde was used in the reaction, the dichlorinated derivative **5b** was isolated in 90% yield without further purification. Esterification of benzoic acid **5a** using an excess of 1,14-dibromotetradecane [18] (2.5 eq) afforded ester **6a** after silica chromatography. The same protocol was used to synthesize **6c** starting from the 70/30 mixture of **5b**/**5c** obtained in the previous step. In this way, the mono-chlorinated analogue **6c** was

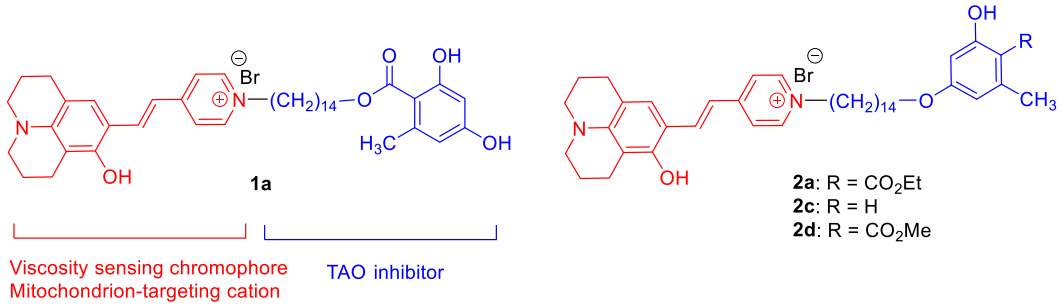

Fig. 1. Structures of fluorescent TAO inhibitor conjugates **1a**, **2a**, **2c**, and **2d** bearing a molecular rotor as viscosity sensor (in red) and a TAO inhibitor pharmacophore (in blue).

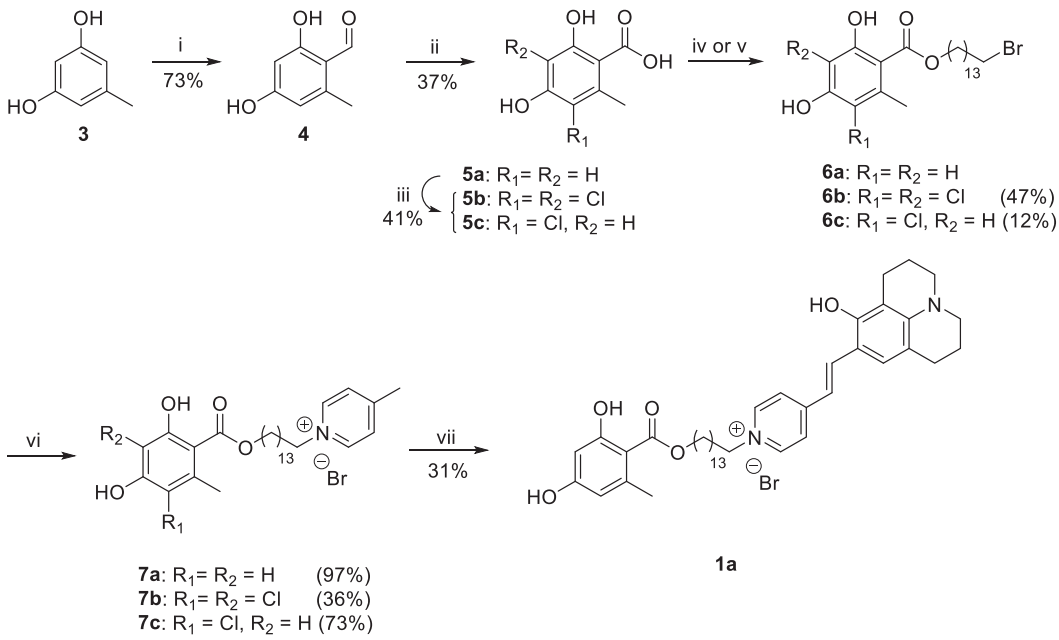

Scheme 1. Synthesis of julolidine derivative **1a** and chloro intermediates **7b**,**c**.
Reagents and conditions: (i) $POCl_3$, DMF, r.t, 18 h; (ii) $NaClO_2$, Na_2HPO_4, DMSO/H_2O, 0 °C then r.t, 18 h; (iii) H_3NSO_3, CH_2O, $NaClO_2$, H_2O/THF, 0 °C, 20 min; (iv) 1,14-dibromotetradecane, $NaHCO_3$, CH_3CN, 80 °C, 72 h (**5a** and **5c**); (v) 14-bromotetradecan-1-ol [19] Ph_3P, DIAD, THF, 0→rt, 3 h (**5b**); (vi) 4-methylpyridine, CH_3CN, 80 °C, 3 days; (vii) 9-Formyl-8-hydroxyjulolidine, pyridine, 70 °C, 24 h.

isolated in low yield (12%) by silica chromatography. Compound **6b** was synthesized with 47% yield from **5b** to 14-bromotetradecan-1-ol [19] using the Mitsunobu protocol. Quaternary pyridinium salts intermediates **7a-c** were produced in quantitative yields after 3 days of reaction with 4-methylpyridine. Finally, Knoevenagel condensation between **7a** and 9-formyl-8-hydroxyjulolidine yielded the target compound **1a** incorporating the julolidine-based viscosity sensor. This last reaction, which is low yielding (typically 20–30%), was a limiting step of this synthetic route. We found that the best results were obtained with 0.6–0.7 eq of piperidine, EtOH as solvent, working at 65–70 °C. The reaction time should not exceed 2 days to avoid degradation of the product and promotion of other by-products. Hence, part of the starting material was recovered during the purification step.

Finally, due to the difficulties encountered with the selective chlorination of 2,4-dihydroxy-6-methylbenzoic acid (**5a**), the synthesis of the mono-chlorinated analogue of **1a** (R_1 = Cl, R_2 = OH) was dropped. However, the biological activity of the chlorinated intermediates was determined (Table 1) to complement the structure-activity relationships (SAR) of these series.

Table 1
Photophysical properties of **1a**.

Solvent	Φ_F[a]	Tau (ns)[b]
Water	0.0013 ± 0.0005	0.065 ± 0.007
EtOH	0.0057 ± 0.0006	0.077 ± 0.002
EtOH:Glycerol 8:2	0.0094 ± 0.0004	0.097 ± 0.002
EtOH:Glycerol 1:1	0.027 ± 0.002	0.175 ± 0.002
EtOH:Glycerol 3:7	0.049 ± 0.007	0.26 ± 0.03
EtOH:Glycerol 2:8	0.080 ± 0.010	0.36 ± 0.06
EtOH:Glycerol 1:9	0.129 ± 0.019	0.47 ± 0.09
Glycerol	0.137 ± 0.010	0.59 ± 0.15

[a] Calculated using two different concentrations and two different excitation wavelengths. The employed reference was Rhodamine 101 (in EtOH).
[b] Fluorescence lifetimes are amplitude-weighted average values from tri-exponential decay functions, globally fitted to five experimental decay traces obtained with λ_{ex} = 530 nm and at the emission wavelengths 570, 590, and 610 nm.

In order to obtain a carboxylic group in the pharmacophore, the strategy was modified so that the C14 methylene chain is grafted to OH in position 4 via Mitsunobu reaction [9]. The synthetic pathway leading to compounds **2a-d** is depicted in Scheme 2. Compound **8** was synthesized from ethyl 2,4-dihydroxy-6-methylbenzoate and bromotetradecan-1-ol using the Mitsunobu protocol as reported [9]. Reaction of **8** with 4-methylpyridine in refluxing CH_3CN gave the quaternary pyridinium salt **9** (71%). Saponification of **9** with 3.5 M KOH at 50 °C yielded the carboxylic acid **10** in 72% yield. Knoevenagel condensation between 9-formyl-8-hydroxyjulolidine and **9** yielded the expected ethyl ester target compound **2a** (21%). In contrast, Knoevenagel condensation between 9-formyl-8-hydroxyjulolidine and **10** gave the decarboxylated by-product **2c** instead of **2b**. The methyl ester **2d**, obtained from **2a** by trans-esterification with MeOH in aqueous KOH, was isolated by preparative HPLC whereas **2b** could not be isolated in pure form.

The julolidine molecular rotor lacking the TAO pharmacophoric moiety (compound **12**) was synthesized in two steps from 4-methylpyridine (Scheme 3). The low yield (7%) of the second step of this synthesis was attributed to the formation of the 4-methyl-1-(14-(piperidin-1-yl)tetradecyl)pyridin-1-ium by-product.

2.2. Photophysical characterization of TAO inhibitor conjugates

Compounds **1a** and **2a**–**d** incorporate the same molecular rotor in their structure, separated from the TAO pharmacophore by a C14 methylene linker. Hence, they should display similar photophysical properties. Therefore, only the photophysical properties of **1a** were characterized in detail. For comparison, the photophysical properties of **2a** are given in Table S1.

Emission properties are sensitive to viscosity changes. Compound **1a** holds a typical D–π–A chromophore structure, which usually results in marked solvatochromic behavior due to polar solvents stabilizing the excited-state through dipole–dipole interactions and hydrogen bonding [20]. Even more important is the

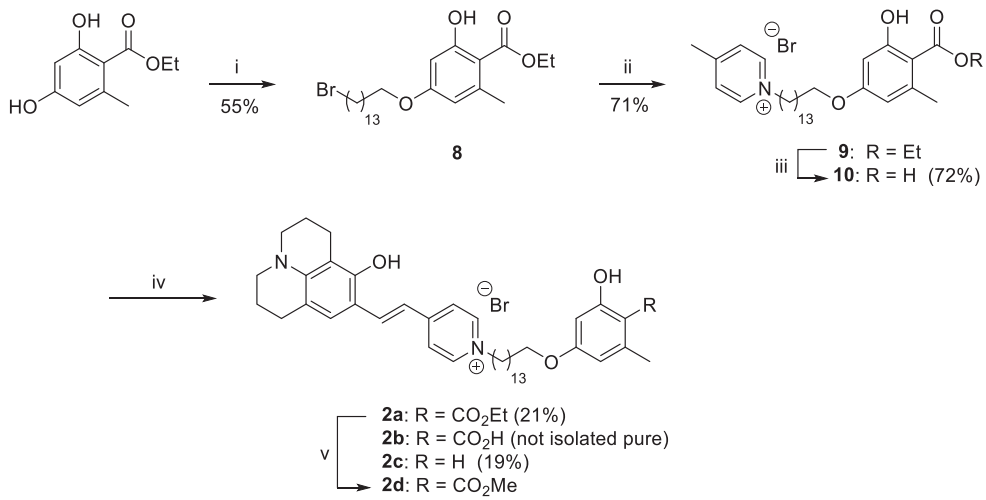

Scheme 2. Synthesis of julolidine derivatives **2a-d**. Reagents and conditions: (i) DIAD, PPh_3, HO–$(CH_2)_{14}$–Br, THF, r.t., 18 h; (ii) 4-methylpyridine, CH_3CN, 80 °C, 3 days; (iii) 1) 3.5 M KOH, H_2O/MeOH (2/1), 50 °C, 48 h, 2) 3.5 M HCl; (iv) 9-formyl-8-hydroxyjulolidine, pyridine, 75 °C, 24 h; (v) KOH, H_2O/MeOH, r.t., 24 h.

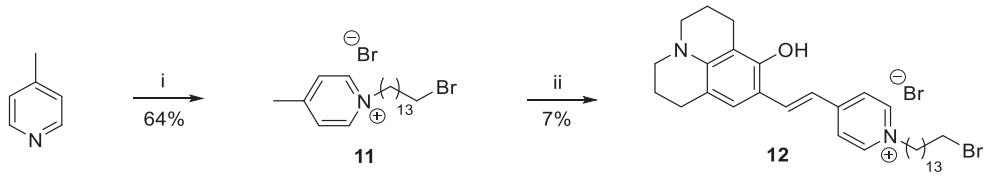

Scheme 3. Synthesis of compound **12**. Reagents and conditions: (i) Br–$(CH_2)_{14}$–Br, CH_3CN, 48 h; (ii) 9-Formyl-8-hydroxyjulolidine, piperidine, 75 °C, 24 h.

fact that the HJVPI moiety behaves as a common rotor fluorophore, thus exhibiting viscosity dependence of its photophysical properties [12]. The absorption spectrum in the visible range, attributed to the HJVPI rotor, showed a maximum ranged from circa 540 nm in organic alcohols to 620 nm in water, and usually exhibiting dual-band absorption (Figure S1 in the Supplementary Materials). The fact that the spectrum is clearly blue-shifted in organic alcohols indicated a specific interaction with hydroxyl groups. Interestingly, a change in the absorption spectrum was observed when different amounts of glycerol (ranging from 1 to 20%) were added to a solution of **1a** in H_2O (Figure S2). This behavior was ascribed to the conformational switch from a twisted structure ($\lambda_{max} = 540$ nm) to a planar form of **1a** ($\lambda_{max} = 620$ nm), probably caused by steric hindrance of the hydrogen bonds between organic alcohols and the HJVPI hydroxyl group. This steric hindrance makes the twisted structure more stable in alcohols, whereas in water, a small molecule, the planar structure is more stable in the ground state.

Importantly, the rotor behavior of the HJVPI chromophore resulted in a large dependence of the emission properties with the environment viscosity. Fast rotation of the fluorophore in the excited state resulted in low fluorescence emission efficiency of **1a** as evidenced in water and EtOH (see Table 1).

In contrast, as expected for a molecular rotor-based fluorophore, the fluorescence properties of **1a** were sensitive to the viscosity of the environment as evidenced in the emission spectra of **1a** in different mixtures EtOH:glycerol, gathered in Fig. 2. The emission quantum yield, Φ_F, of **1a** was enhanced 24-fold in more viscous systems containing a higher proportion of glycerol (from 0.006 in 8:2 EtOH to 0.14 in pure glycerol). The enhancement with solvent viscosity in the average fluorescence lifetime ranged from 77 ps in EtOH to 590 ps in pure glycerol (Table 1). In any case, these average lifetime values represent fast deactivation dynamics, composed by

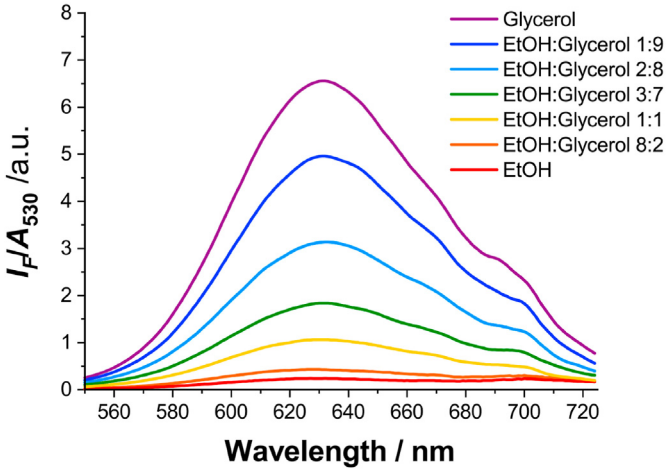

Fig. 2. Emission spectra of **1a** (normalized by the absorbance at the excitation wavelength, $\lambda_{ex} = 530$ nm) in EtOH:glycerol mixtures.

three different exponential components. Interestingly, in the red-edge of the emission band, the short decay time exhibited negative pre-exponential factors in high viscosity mixtures, indicating the presence of excited-state dynamics in which the more fluorescent form is formed. This was also supported by a slight spectral shift in the emission maximum from 627 nm in EtOH to 632 nm in glycerol. The marked change in the fluorescence of **1a** was attributed to the geometry relaxation to a state with substantial intramolecular charge transfer (see more details in Computational Results section) [21].

Given that the fluorophore part of molecules **2a-d** is the same

than that in **1a**, similar results are expected for the other compounds. Indeed, **2a** exhibited very similar photophysical properties to **1a** in water, ethanol and ethanol:glycerol mixtures (Table S1, Figure S3).

The fluorescence studies of **1a** and **2a** recorded in glycerol–ethanol mixtures agree with the interconverting 'twisted' and 'planar' conformers [22] of compound **1a**, respectively. In organic alcohols, such fluorophore undergoes [23] fast intramolecular electron transfer from the donor to the acceptor part of the molecule. This electron transfer is accompanied by intramolecular D–A twisting around the single bond (Fig. 3) and produces a relaxed perpendicular structure.

2.3. Ab initio calculations

The optimized geometries of **1a** obtained at B3LYP/6-31 + G** level of theory for the ground (a) and excited (b) states are shown in Fig. 4 and Table S2. DFT calculations give a slightly twisted ($\phi_2 = 17°$) optimized geometry for the ground state whereas a larger dihedral angle ($\phi_2 = 90°$) between the julolidine and the pyridinium salt is found in the excited state. In addition, the angle α for C7–23C–C24 is slightly different from the ground state to the excited state (130° and 122° respectively). Of note is the shorter C4–C7 bond length in the excited state, as a result of the favored charge transfer (CT) from the nitrogen of the julolidine moiety to the pyridinium group (Table S2).

Further mechanical computations were conducted to investigate the role of frontier molecular orbitals (FMO) crucial to understand and acquire information about the molecule after excitation. As shown in Figure S4, the HOMO electronic distribution of **1a** is mainly located on the julolidine core whereas the electron density of the LUMO/LUMO+1 is localized on the electron withdrawing pyridinium group, which indicates effective charge transfer from donor to acceptor group. The major contribution to the transition bands involves the excitation from HOMO-1 to LUMO (coefficient value ~ 0.65) and the minor contribution HOMO-LUMO (coefficient value ~ 0.65).

2.4. Biological activity

The trypanocidal activity of the fluorescent probes **1a** and **2a-d** was determined in vitro against wild type (s427) and drug resistant strains of *T. brucei* (i.e. B48, AQP1-3 KO) with a resazurin-based assay [9,10]. The EC_{50} values ranged from 0.5 to 1.0 μM against WT parasites with selectivity indices over mammalian cells ranging from 29 to >100 (Table 2). Importantly, the compounds were equipotent against the multi-drug resistant strain B48 that lacks the P2/TbAT1 and High Affinity Pentamidine Transporter (HAPT1) drug transporters ($P > 0.05$ by Student's unpaired *t*-test) [24]. Interestingly, however, several of the analogues were significantly ($P < 0.05$, $P < 0.01$) more active against a strain lacking all three *T. b. brucei* aquaporins [25], indicating potential sensitization under conditions where glycerol, a metabolic waste product in *T. b. brucei* [26], accumulates to higher levels in the cell. The reference drug pentamidine displayed resistance factors (RF) of 102 and 6.9 for B48 and AQP1-3 KO, respectively ($P < 0.001$). Pentamidine is transported by both P2/TbAT1 [27] and HAPT1, the latter of which has been identified as TbAQP2 [28].

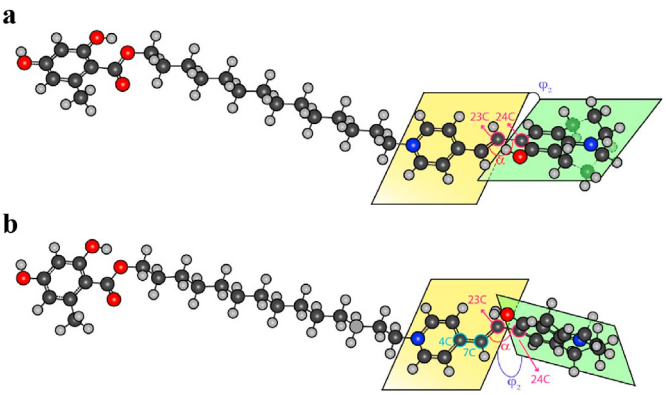

Fig. 4. Optimized (a) ground excited state (S_0) and (b) first excited state (S_1) structures. The julolidine in the ground state minimum is almost planar with $\phi_2 = 17°$. The long axis of the molecular rotor is almost straight and is bent with an angle $\alpha = 130°$. In the first excited state, the molecular rotor is twisted $\phi_2 = 90°$ between the donor and the acceptor with an angle $\alpha = 122°$.

As regards to enzyme inhibition, the carboxylate probes **2a-d** were more potent inhibitors of recombinant TAO ($IC_{50} = 1.6–145$ nM) than the benzoate derivative **1a** (360 nM). The higher inhibitory potency of ethyl and methyl ester substituents (**2a**, **2d**) vs H (**2c**) agreed with the SAR results observed previously for analogous series lacking the fluorescent julolidine-based viscosity sensor [9]. This could indicate that these compounds bind to TAO in a similar fashion.

The charge delocalization of the cationic moiety seemed to play a role in TAO inhibition as shown by the micromolar IC_{50} values of the pyridinium intermediates (**7a**, **10**) compared to the submicromolar inhibition displayed by the julolidine-based compounds (**1a, 2a-d**) or the triphenylphosphonium and quinolinium analogues reported before (Chart 1) [9,10]. In line with previous reports [8,29,30], the addition of one (**7c**) or two chlorine atoms (**7b**) in the TAO-binding pharmacophore enhanced TAO inhibition (**7c** ≈ **7b** > **7a**). However, and unexpectedly, the addition of chlorine atoms correlated negatively with the activity against *T. brucei* (**7b** < **7c** < **7a**). Since **7a** is the most cytotoxic compound of the series ($CC_{50} = 0.76$ μM), the observed nanomolar trypanocidal effect could be due, to some extent, to unspecific toxicity upon accumulation to high levels into trypanosomes.

As expected, the julolidine derivative **12** lacking the 2,4-dihydroxy-6-methylbenzoic acid pharmacophore did not inhibit TAO although it showed submicromolar activity against *T. brucei* (Table 2). Compound **12** holds the lipophilic pyridino-julolidine conjugated cation like **1a**, **2c**, and **2d**; thus, the observed activity possibly reflects a different mechanism of action via other mitochondrial targets of *T. brucei*. For the whole series, it is expected that accumulation of these compounds in the *T. brucei* mitochondrion will affect the mitochondrial membrane potential Ψ_m because of

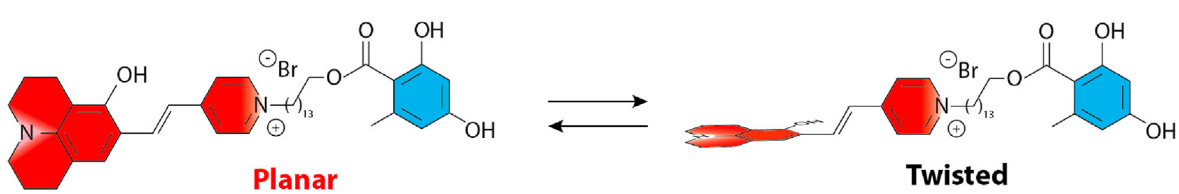

Fig. 3. Twisted and planar conformations of compound **1a**.

Table 2
Biological activity of fluorescent TAO inhibitor conjugates **1a** and **2a**–**d**, and synthetic intermediates **6c**, **7a-c**, **10** and **12**: in vitro activity against *T. brucei* wild-type (WT) and drug-resistant lines, cytotoxicity against mammalian cells, and inhibition of TAO.

	T. b. brucei EC_{50} (μM)					Cytotoxicity CC_{50} (μM)		rTAO IC_{50} (μM)[g]
Cmpd	S427 (WT)[a]	B48[b]	RF[c]	AQP1-3 KO[d]	RF[c]	HEK[e]	SI[f]	
1a	1.01 ± 0.04	1.19 ± 0.05	1.17	1.048 ± 0.050	1.03	>100	>100	0.36 ± 0.07
2a	0.80 ± 0.05	0.85 ± 0.05	1.07	0.663 ± 0.054	0.83	23.3 ± 0.1	29.1	0.0016 ± 0.0002
2c	0.50 ± 0.07	0.63 ± 0.05	1.25	0.43 ± 0.05	0.85	22.2 ± 2.2	44.1	0.145 ± 0.015
2d	0.54 ± 0.02	0.59 ± 0.01	1.10	0.44 ± 0.04	0.81	23.6 ± 1.5	43.6	0.042 ± 0.02
12	0.43 ± 0.01	0.49 ± 0.04	1.16	0.34 ± 0.02*	0.79	26.7 ± 0.6	62.6	>5
6c	6.84 ± 0.60	10.1 ± 0.9	1.48	13.1 ± 0.3**	1.91	55.9 ± 0.7	8.2	0.75 ± 0.19
7a	0.055 ± 0.008	0.06 ± 0.01	1.04	NT[h]		0.76 ± 0.14	13.8	>5
7b	2.55 ± 0.17	2.64 ± 0.18	1.03	NT		4.4 ± 0.5[i]	1.7	0.91 ± 0.08
7c	0.24 ± 0.05	0.22 ± 0.04	1.53	0.19 ± 0.02	0.80	43.7 ± 2.7	182	0.72 ± 0.20
10	19.7 ± 0.4	23.3 ± 0.8	1.18	16.6 ± 0.9*	0.84	>200	>10	1.80 ± 0.13
Pentamidine	0.0049 ± 0.0004	0.50 ± 0.05	102	0.034 ± 0.03	6.9			
Phenylarsine oxide						0.46 ± 0.04		

*, $P < 0.05$ and **, $P < 0.01$ from WT control EC_{50} by Student's unpaired *t*-test; n = 3.
[a] Trypomastigotes of *T. b. brucei* s427 (n ≥ 3).
[b] *T. brucei* cell line from which the *TbAT1* gene was knocked out, followed by in vitro adaptation to pentamidine [24].
[c] Resistance factor relative to WT.
[d] *T. brucei* cell line from which *all* aquaporins were knocked out [25] (n ≥ 3).
[e] Cytotoxicity on human embryonic kidney cells (n = 3).
[f] Selectivity index (SI) = CC_{50}/EC_{50} (*T. brucei* WT).
[g] Purified recombinant trypanosome alternative oxidase (ΔMTS-TAO) [10] from *T. b. brucei* (n = 3).
[h] Not tested.
[i] Partial inhibition.

the (1) accumulation of cations in the mitochondrial matrix and (2) disruption of mitochondrial functions involved in maintaining the ion gradients. Similar effects have been shown for various diamidines [31], choline-derived dications [32], phenanthridines [33] and bisphosphonium compounds [34,35]. The latter were shown to act on the mitochondrial F_oF_1 ATPase of *T. brucei* [36]. Consequently, the lack of correlation between TAO inhibition and efficacy against *T. brucei* of this series is probably the consequence of various factors including multi-target activity.

2.4.1. Real-time monitoring of TAO inhibitor accumulation

In our previous reports on the trypanocidal effects of TAO inhibitors it was never possible to monitor the rate at which the drug is accumulated in the trypanosome. However, the coupling to the julolidine fluorophore allowed us to monitor the concentrative uptake into the cells in real-time, using a fluorimeter. Fig. 5A shows that the uptake of compound **2a** was very rapid, eliciting a detectable signal immediately after uptake. It was also dose-dependent, as at 0.2 μM the fluorescence increased by 3.86 A U./min and at 2 μM the rate was 33.04 A U./min by linear regression (average of triplicate). As **2a** is a potent inhibitor of TAO, this strong fluorescence might in part result from the production of glycerol that TAO inhibition is known to engender. To separate the signal of the accumulation from the extra fluorescence associated with any changes in viscosity, we utilized an identical probe without the TAO pharmacophore head group, **12**, which we allowed to accumulate for 1 h followed by the application of a known TAO inhibitor, TAO38 or TAO47 (Table S3) [10], followed by a further recording of 1 h (Fig. 5B). Neither inhibitor affected the fluorescence relative to the control (same volume of PBS pH7.4).

However, the glycerol that is produced after inhibition of TAO derives from the de-phosphorylation of Glycerol-3-phosphate by glycerol kinase [37], which is located in the glycosomes [38]. The glycerol so produced is believed to escape to the cytosol, from which it is released as a waste product to the extracellular environment, via aquaglyceroporins (AQPs) [39], and no passive diffusion of glycerol can be detected across the *T. brucei* cell membrane [28]. As such, the experiment was repeated with a *T. b. brucei* strain from which all three AQP-encoding genes were deleted (aqp1-3 *null*) and which is extra sensitized to TAO inhibitors [25]. However, Fig. 5B reveals no difference between the fluorescence of aqp1-3 *null* cells incubated with **12** in the presence of TAO38 or TAO47 or the same volume of PBS. As even the addition of 10 mM glycerol to the culture medium failed to elicit a significant fluorescence response ($P > 0.05$ for both strains), we conclude that the metabolite is very effectively excluded from entering the mitochondrion. This is consistent with the latest insights into *T. brucei* mitochondrial metabolism, as there is no known metabolic role for glycerol in the mitochondrion, and no known mitochondrial carrier for it. Moreover, although cardiolipin biosynthesis, which is essential in *T. brucei* [40,41], is finalized inside the mitochondrion, the glycerol-utilising step is conducted in the cytosol [42].

2.5. Fluorescence imaging in live cells

2.5.1. One/two-photon excitation fluorescence microscopy in human preosteoblast cells

An important step in the biological activity of TAO inhibitors is that their activity concentrates in the mitochondria. Hence, the chimeric design of compounds **1a** and **2a-d** allows direct imaging of the localization of the drug at a cellular and/or microorganism level.

First, we tested the feasibility of **1a**, **2a** and **2c** for 1- and 2-photon absorption fluorescence imaging in live cells, and studied colocalization with mitochondria, using different commercial mitochondria trackers (MitoTracker Green, MTG, or MitoTracker Deep Red, MTDR).

For single-photon excitation fluorescence imaging, we used dual-color fluorescence microscopy, allowing pulsed-interleaved excitation with 561-nm and 640-nm lasers [43]. This configuration permits 2-color colocalization studies avoiding spectral crossover due to direct excitation of one dye into the other detection channel. For these experiments, we excited **1a**, **2a** and **2c** with the 561-nm laser whereas we used MTDR, excited with the 640-nm laser, for mitochondria imaging. Fig. 6 shows that the three compounds exhibited a good mitochondrial localization, with average Pearson coefficients of 0.7 ± 0.1, 0.5 ± 0.1, and 0.40 ± 0.05 for **1a**, **2a** and **2c**, respectively. Figures S5, S6, and S7 in the Supplementary Material shows further examples of colocalization of the three dyes.

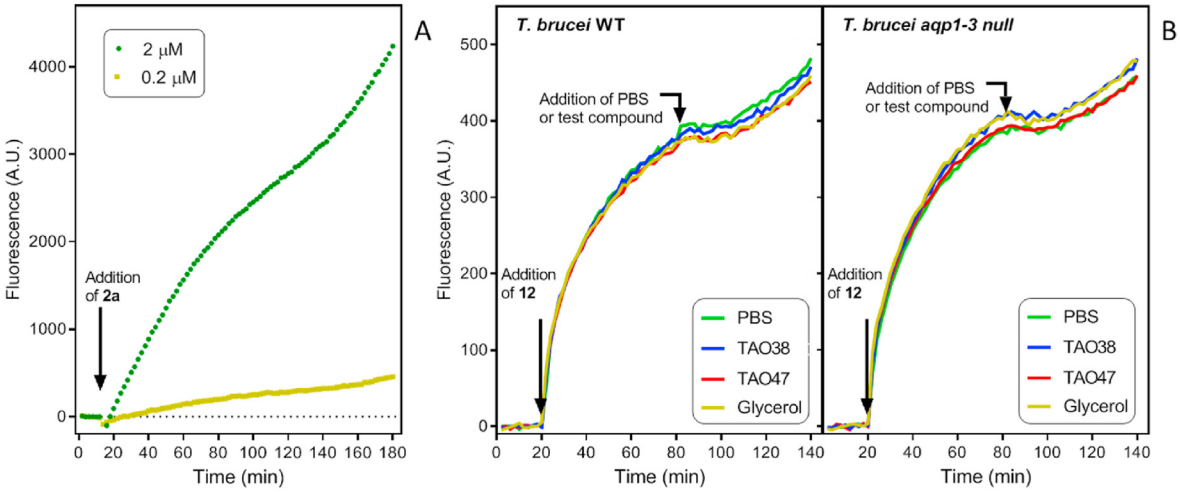

Fig. 5. Real-time monitoring of fluorescence in *T. b. brucei* bloodstream forms. A. Fluorescence of *T. b. brucei* s427WT incubated with **2a**, added to the indicated concentrations at 14 min into the recording. B. Fluorescence of **12**, added at 20 min to a final concentration of 0.2 μM, was recorded in parallel for strain 427WT and *aqp1-3 null*, on the same plate. At 80 min, 20 μL of PBS pH 7.4, 100 mM glycerol/PBS or of 2 μM TAO38 or TAO47 in PBS was added to the appropriate wells. Every trace is the average of 3 replicate wells on the same plate.

We also tested compound **1a** in colocalization studies with mitochondria using two-photon excitation microscopy (see Experimental section for details). Multi-photon excitation is a nonlinear phenomenon that enhances resolution of fluorescence images by reducing the excitation cross-section, reduces background, and allows for deeper penetration of the excitation light in tissues, since near infrared radiation is employed. For these experiments, we used 850-nm excitation radiation, suitable for simultaneously exciting the mitochondrial tracker MTG and **1a**. Fig. 7 confirms the excellent mitochondrial localization of the dye (Pearson coefficient of 0.74 ± 0.07, as well as its suitability for two-photon absorption imaging.

2.5.2. Quantification of accumulation in mitochondria

To confirm mitochondrial accumulation, we also quantified the partition of **1a** in functional isolated rat liver mitochondria using fluorescence spectroscopy [44]. By comparing the absorption and fluorescence emission of **1a** in the supernatant after partition in extract containing functional mitochondria and subsequent separation by centrifugation and washing (see Experimental section for details), we estimated that 66 ± 20% of the total was delivered into rat liver mitochondria. This confirms an efficient partition of the dye in such organelles. We could not perform similar experiments with the other dyes because of their very low quantum yield in water, so that the associated error in measuring the fluorescence emission in the supernatants was very large.

2.5.3. Fluorescence microscopy in T. brucei

To attest the localization of the drug in *T. b. brucei*, live parasites were imaged using a high-resolution microscope. Cells were immobilized with PBS-primed CyGEL, using MTG to stain the parasite's single mitochondria and Hoechst 33,342 to stain DNA (the nucleus and the mitochondria). Compound **1d** was observed to stain the same structure as the MTG, confirming the mitochondrial localization of **1d** in live trypanosomes (Fig. 8).

3. Conclusions

Three fluorescent TAO inhibitors with submicromolar activity against *T. brucei* were synthesized and their photophysical properties were determined. The inhibitors, which accumulate specifically in the mitochondria of mammalian and trypanosome cells, are fluorescent probes that are sensitive to the viscosity of the milieu. They show a high SNR in one and two photon absorption spectroscopy. The lack of a detectable increase in fluorescence with this probe upon inhibition of TAO shows that the *T. brucei* mitochondrial membrane is impervious to glycerol, consistent with current models of its metabolism.

4. Experimental part

4.1. Chemistry

Anhydrous solvents were purchased to ACROS Organics in AcroSeal® bottles and used as received. Thin Layer chromatography (TLC) was performed on silica gel 60 F254 aluminum TLC plates (MERCK). Chromatography was performed on silica gel 60 (0.040–0.063 mm, 230–400 mesh ASTM, MERCK). LC-MS spectra were recorded on a WATERS apparatus integrated with a HPLC separation module (2695), PDA detector (2996) and Micromass ZQ spectrometer using electrospray ionization (ES^+). Analytical HPLC was performed with a SunFire C18–3.5 μm column (4.6 mm × 50 mm). Mobile phase A: CH_3CN + 0.08% formic acid and B: H_2O + 0.05% formic acid. UV detection was carried over 190–440 nm. Accurate mass were measured with an Q-TOF 6520 spectrometer (Agilent Technologies) using electrospray ionization. ^1H NMR and ^{13}C NMR spectra were registered on a Bruker Avance-300, Varian Inova-400, Varian-Mercury-400, and Varian-500. Chemical shifts of the ^1H NMR spectra were referenced to the residual peak of the deuterated solvent: δ 7.26 ppm ($CDCl_3$), 3.31 ppm (Methanol-d_4), and 2.50 ppm (DMSO-d_6). Chemical shifts of the ^{13}C NMR spectra were referenced at 77.16 ppm ($CDCl_3$), 49.0 ppm (CD_3OD), and 39.5 ppm (DMSO-d_6). Peak multiplicities are defined as follows: br (broad peak), s (singlet), d (doublet), t (triplet), q (quadruplet), p (quintuplet), m (multiplet), and combinations of the same. Coupling constants *J* are given in hertz (Hz). Melting points were measured with a Reichert-Jung Thermovar apparatus and are uncorrected. All of the biologically tested compounds were ≥95% pure by HPLC.

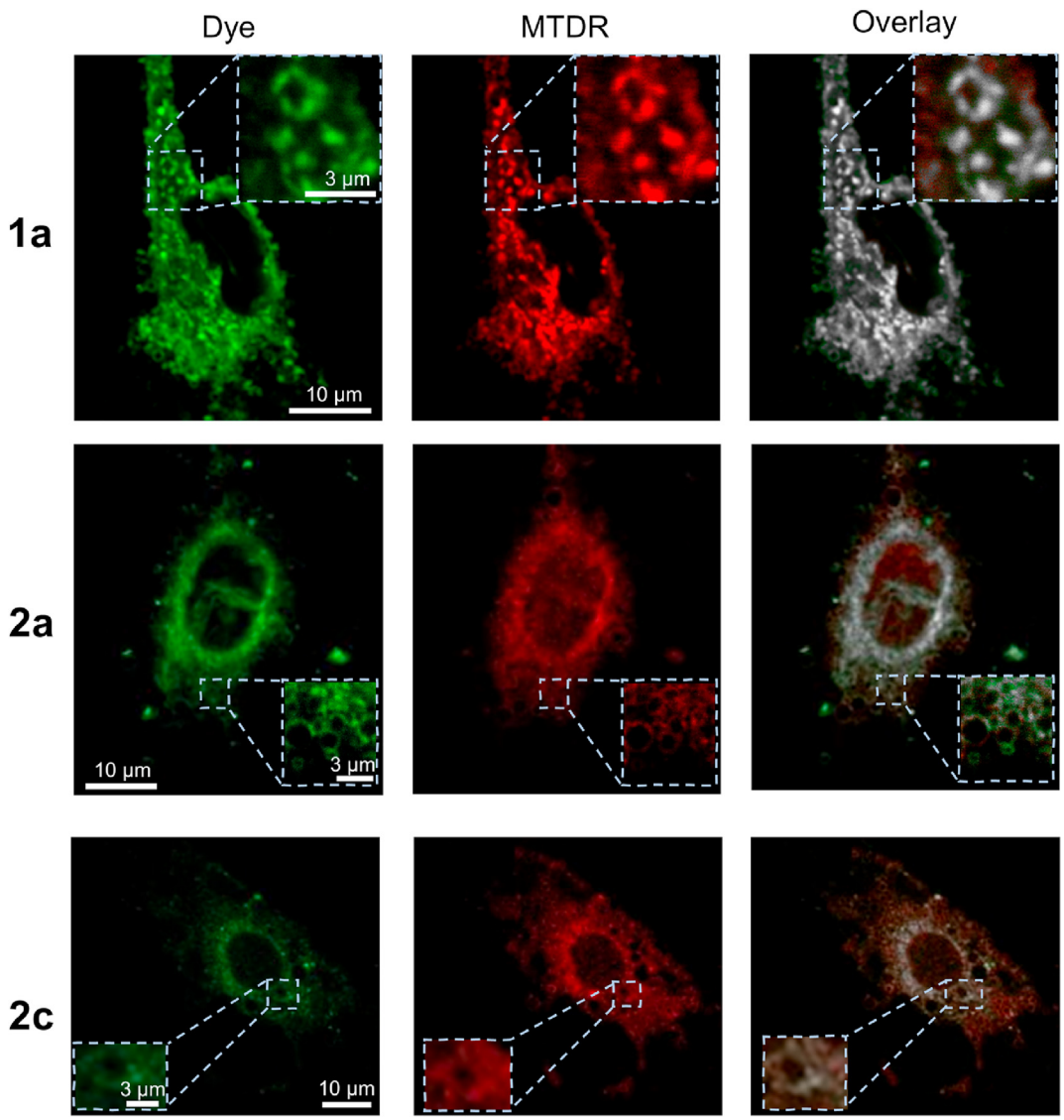

Fig. 6. Colocalization experiments between compounds **1a**, **2a** and **2c** (green channel) and MTDR as mitochondrial tracker (red channel) in the preosteoblast cell line MC3T3-E1 using single-photon excitation fluorescence microscopy. The overlay images show colocalized pixels in white. Insets represent zoomed sections of the overall images.

4.2. Synthesis protocols

2,4-dihydroxy-6-methylbenzaldehyde (4). Compounds **4** and **5a** were synthesized following a reported procedure [45]. A solution of orcinol (6.9 g, 55.6 mmol) in anhydrous DMF (23 mL) was added slowly to a stirred solution of phosphorous oxychloride (10.4 mL, 110 mmol) in anhydrous DMF (26 mL) cooled down to 10 °C. Then, the reaction mixture was kept under stirring 18 h at room temperature. The flask was cooled with an ice-bath and the reaction was cautiously quenched with cold water (150 mL) and basified to pH ≈ 10 with 10% aqueous NaOH solution. The reaction mixture was heated to reflux for 10 min, cooled to room temperature, and acidified to pH 1 with concentrated HCl. The yellowish precipitate was collected by filtration, washed with water and dried under vacuum to give **4** as pale yellow powder (6.2 g, 73%). ^{1}H NMR (300 MHz, DMSO-d_6) δ (ppm): 2.45 (s, 3H), 6.12 (d, J = 3.0 Hz, 1H), 6.20 (d, J = 3.0 Hz, 1H), 10.05 (s, 1H), 10.68 (br, 1H), 12.05 (brs, 1H).

2,4-dihydroxy-6-methylbenzoic acid (5a). To a solution of **4** (1.0 g, 6.6 mmol) and NaH_2PO_4 (1.97 g, 16.4 mmol) in DMSO (21 mL) and water (4.5 mL) at 0 °C was slowly added a solution of $NaClO_2$ (1.48 g, 16.4 mmol) in water (4.5 mL). The reaction mixture was stirred at room temperature for 48 h. The reaction mixture was basified with aqueous K_2CO_3 and extracted with EtOAc. The aqueous phase was acidified to pH = 1 with 37% HCl, then it was extracted with EtOAc (3 ×). The organic phase was dried ($MgSO_4$) and the pure product was isolated by crystallization from a mixture of 30% AcOH in water. Off-white solid (386 mg, 37%). HPLC (UV) > 95%. ^{1}H NMR (300 MHz, DMSO-d_6) δ 2.39 (s, 3H), 6.11 (s, 1H), 6.17 (s, 1H), 10.13 (brs, 1H), 12.06 (br, 1H). LRMS (ESI$^-$) m/z 167 $(M - H)^-$.

3,5-dichloro-2,4-dihydroxy-6-methylbenzoic acid (5b). Under inert atmosphere p-orsellinic acid **5a** (300 mg, 1.8 mmol) and sulfamic acid (871 mg, 8.9 mmol) were suspended in 12 mL of a mixture H_2O/THF (2:1). The mixture was cooled down to 0 °C and freshly purchased acetaldehyde (100 μL, 1.78 mmol) was added. Thereafter, $NaClO_2$ (807 mg, 8.9 mmol) dissolved in H_2O (1 mL) was introduced and the reaction was warm up to room temperature and stirred for 20 min. Then, the mixture was quenched with saturated NH_4Cl aqueous solution (50 mL) and extracted with ethyl acetate (100 mL). The organic layer was dried over $MgSO_4$ and

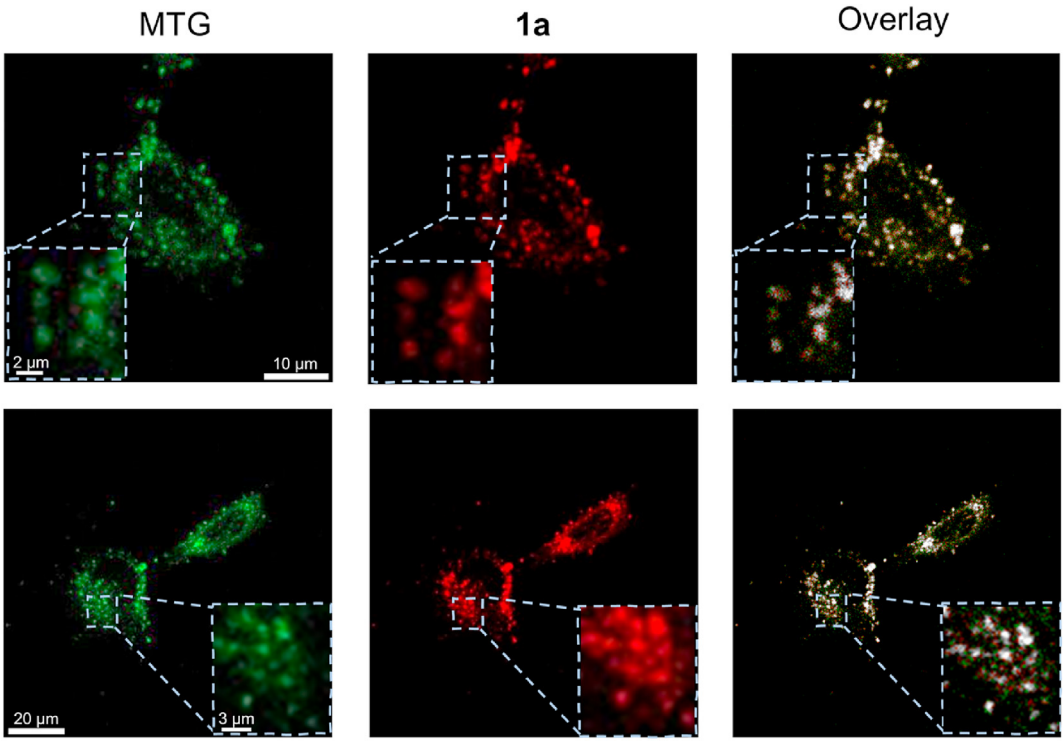

Fig. 7. Two representative images of colocalization experiments between **1a** (red channel) and MTG as mitochondrial tracker (green channel) in the preosteoblast cell line MC3T3-E1 using 850-nm two-photon excitation fluorescence microscopy.

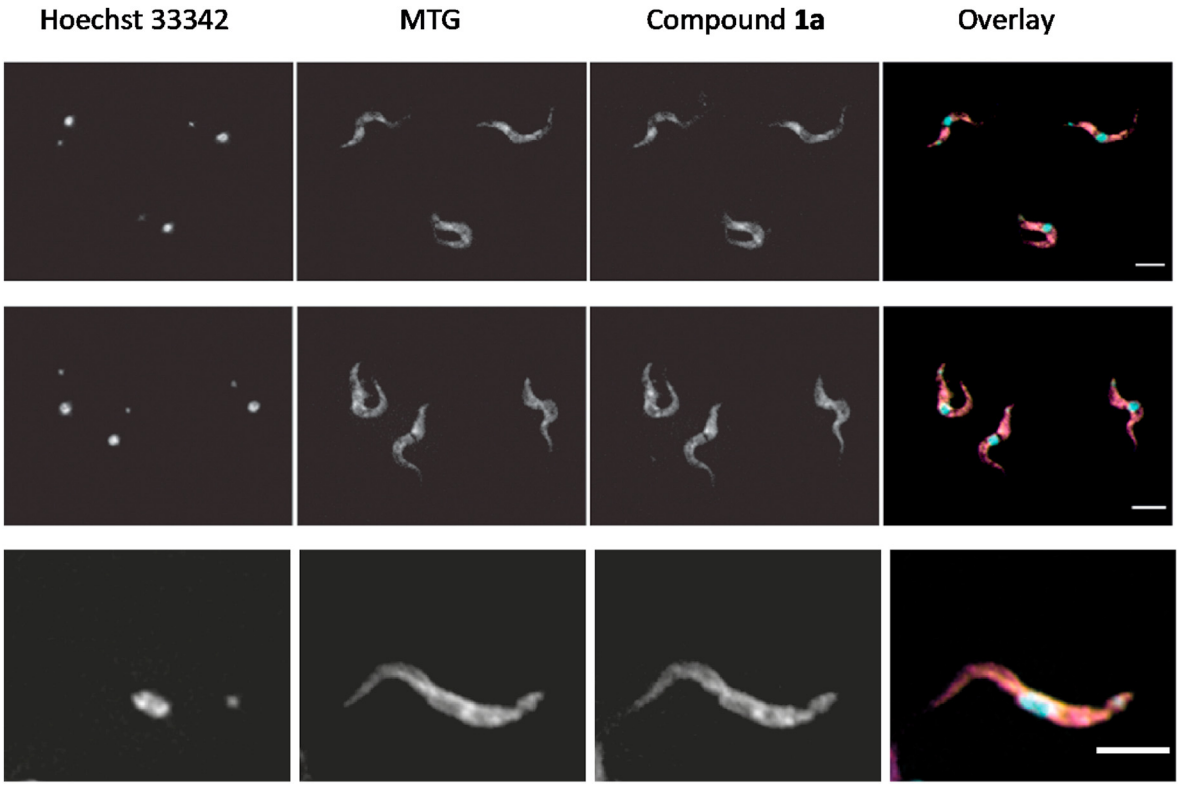

Fig. 8. Mitochondrial localization of **1a** in *T. brucei*. The first column is Hoechst 33342 (stains DNA), the second Mitotracker Green, third compound **1a** and the last one the overlay (Hoechst in cyan, Mitotracker in yellow and **1a** (40 μM, 1 h) in magenta). All scale bars indicate 5 μm.

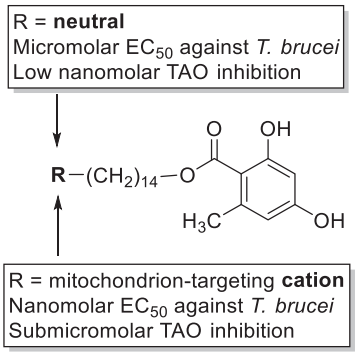

	IC$_{50}$ (μM)	
	T. brucei	rTAO
Br	14.6	0.007
Ph_3P^+	0.0016	0.088
$Quin^+$	0.032	0.104

Chart 1. Example of previous 2,4-dihydroxybenzoate-based TAO inhibitors [8,10]. Ph_3P^+: triphenylphosphonium; $Quin^+$: quinolin-1-ium; rTAO: recombinant TAO enzyme.

concentrated under reduced pressure leading to a pale brown solid (380 mg, 90%) that was used for the next step without further purification. HPLC (UV) > 93%. ^{1}H NMR (400 MHz, Methanol-d_4) δ 2.63 (s, 3H). ^{13}C NMR (100 MHz, Methanol-d_4) δ 174.1, 159.3, 155.0, 138.9, 115.6, 108.2, 108.1, 19.6. ESI-HMRS: *m*/*z* 235.9646[M]$^+$ ($C_8H_6Cl_2O_4$ requires: 235.9643).

14-bromotetradecyl 2,4-dihydroxy-6-methylbenzoate (6a). Compound **6a** was synthesized following a reported procedure [11].

14-bromotetradecyl 3,5-dichloro-2,4-dihydroxy-6-methylbenzoate (6b). Under inert atmosphere, **5b** (44 mg, 0.2 mmol), 14-bromotetradecan-1-ol [19] (50 mg, 0.17 mmol) and PPh_3 (45 mg, 0.19 mmol) were dissolved in THF (3 mL). Then, the reaction was cooled down to 0 °C and DIAD (37 μL, 0.19 mmol) was added. Thereafter, the mixture was warm up to room temperature and was kept under stirring for 2.5 h. The solvent was removed under high vacuum, and the crude solid was purified by flash chromatography column on silica gel (stepwise gradient from 0 to 20% EtOAc in Hexanes). Compound **6b** was obtained as off-white amorphous solid (41 mg, 47%). ^{1}H NMR (300 MHz, $CDCl_3$/Methanol-d_4) δ 1.04–1.33 (m, 20H), 1.56–1.76 (m, 4H), 2.47 (s, 3H), 3.26 (t, *J* = 6.8 Hz, 2H), 4.23 (t, *J* = 6.6 Hz, 1H). ^{13}C NMR (75 MHz, $CDCl_3$) δ 171.2, 158.4, 152.4, 138.0, 114.0, 107. 6, 106.8, 66.8, 34.2, 33.0, 29.7, 29.65, 29.6, 29.3, 28.9, 28.6, 28.3, 26.2, 19.9. ESI-HMRS: *m*/*z*: 510.0932 [M]$^+$ ($C_{22}H_{33}Cl_2O_4$ requires 510.0939).

14-bromotetradecyl 3-chloro-4,6-dihydroxy-2-methylbenzoate (6c). Under inert atmosphere, **5c** (177 mg, 0.88 mmol; used as approximately 70/30 mixture of **5b/5c**) was added to a suspension of $NaHCO_3$ (81 mg, 0.97 mmol) in anhydrous CH_3CN (3 mL).Then, 1,14-dibromotetradecane [18] (806 mg, 2.2 mmol) was added. The reaction was heated up at 80 °C and kept under stirring for one day. After cooling down to room temperature, the solvent was removed under high vacuum. The crude solid was purified by flash chromatography column on silica gel (stepwise gradient from 0 to 20% EtOAc in Hexanes) leading to **6c** (50 mg, 12%) as a pale off-white solid. mp 43–46 °C. ^{1}H NMR (400 MHz, Methanol-d_4) δ 1.28–1.43 (m, 20H), 1.74–1.84 (m, 4H), 2.53 (s, 3H, -C$\underline{H}_3$), 3.41 (t, *J* = 6.8 Hz, 2H), 4.32 (t, *J* = 6.5 Hz, 1H), 6.34 (s, 1H). ^{13}C NMR (100 MHz, Methanol-d_4) δ 171.9, 161.6, 158.7, 139.7, 115.1, 109.5, 102.4, 66.7, 34.4, 34.0, 30.65, 30.61, 30.58, 30.53, 30.49, 30.46, 30.2, 29.8, 29.6, 29.1, 27.2, 19.6. ESI-HMRS: *m*/*z*: 476.1316 [M]$^+$ ($C_{22}H_{34}BrClO_4$ requires 476.1329).

1-(14-((2,4-dihydroxy-6-methylbenzoyl)oxy)tetradecyl)-4-methylpyridin-1-ium bromide (7a). Under inert atmosphere, 14-bromotetradecyl 2,4-dihydroxy-6-methylbenzoate (**6a**) [11] (58 mg, 0.13 mmol) and 4-methylpyridine (15 μL, 0.16 mmol) were dissolved in anhydrous CH_3CN (1.8 mL). The reaction mixture was heated up at 80 °C, and kept under stirring for 3 days. After cooling down to room temperature, a white precipitate appeared. The precipitate was collected by filtration and washed with cold Et_2O to give **7a** (63 mg, 97%) as colorless solid. HPLC (UV) > 95%. mp 118–120 °C. ^{1}H NMR (400 MHz, DMSO-d_6) δ 1.23–1.37 (m, 20H), 1.65–1.69 (m, 2H), 1.83–1.91 (m, 2H), 2.30 (s, 3H, Ors-C$\underline{H}_3$), 2.60 (s, 3H, Pyr-C$\underline{H}_3$), 4.22 (t, *J* = 6.5 Hz, 2H), 4.51 (t, *J* = 7.4 Hz, 2H), 6.15 (d, *J* = 2.3 Hz, 1H), 6.17 (d, *J* = 2.3 Hz, 1H), 7.98 (d, *J* = 6.3 Hz, 2H), 8.92 (d, *J* = 6.8 Hz, 2H), 10.00 (s, 1H), 10.86 (s, 1H). ^{13}C NMR (100 MHz, DMSO-d_6) δ 170.1, 161.6, 161.2, 158.7, 143.7 (N^+-$\underline{C}$H), 140.9, 128.3 (N^+-CH-$\underline{C}$H-), 110.3, 107.1, 100.5, 64.7(-$\underline{C}H_2$-OCO-), 59.9 (-$\underline{C}H_2$-Pyr), 30.5, 28.94, 28.88, 28.85, 28.7, 28.5, 28.3, 28.0, 25.5, 25.3, 22.3 (Ors-$\underline{C}H_3$), 21.3 (Pyr-$\underline{C}H_3$). ESI-HMRS: *m*/*z* 456.3114 [M]$^+$ ($C_{28}H_{42}NO_4$ requires: 456.3114).

1-(14-((3,5-dichloro-2,4-dihydroxy-6-methylbenzoyl)oxy) tetradecyl)-4-methylpyridin-1-ium bromide (7b). Under inert atmosphere, **6b** (25 mg, 49 μmol) and 4-methylpyridine (5.5 μL, 56 μmol) were dissolved in anhydrous CH_3CN (1.5 mL). The reaction was heated up at 80 °C and kept under stirring for 2 days. The solvent was evaporated and the residue was washed several times with hot Et_2O to give **7b** (10.8 mg, 36%) as pale brownish solid. HPLC (UV) > 95%. mp 126–130 °C. ^{1}H NMR (300 MHz, Methanol-d_4) δ 1.29–1.76 (m, 20H), 1.76–1.81 (m, 2H), 1.96–2.01 (m, 2H), 2.53 (s, 3H), 2.67 (s, 3H), 4.38 (t, *J* = 6.5 Hz, 2H), 4.55 (t, *J* = 7.5 Hz, 2H), 7.93 (d, *J* = 6.1 Hz, 2H), 8.80 (d, *J* = 6.2 Hz, 2H). ^{13}C NMR (100 MHz, Methanol-d_4) δ 171.6, 161.3, 157.2, 154.6, 144.8, 137.4, 129.9, 115.6, 110.4, 108.5, 67.3, 62.2, 32.4, 30.65, 30.60, 30.56, 30.51, 30.47, 30.45, 30.12, 30.09, 29.5, 27.2, 27.1, 22.0, 19.5. ESI-HMRS: *m*/*z* 524.2323 [M]$^+$ ($C_{28}H_{40}Cl_2NO_4$ requires 524.2334).

1-(14-((3-chloro-4,6-dihydroxy-2-methylbenzoyl)oxy)tetradecyl)-4-methylpyridin-1-ium bromide (7c). Under inert atmosphere, **6c** (40 mg, 84 μmol) and 4-methylpyridine (10 mL, 0.10 mmol) were dissolved in anhydrous CH_3CN (1.8 mL). The reaction mixture was heated up at 80 °C, and kept under stirring for 3 days. After cooling down to room temperature, a white precipitate appeared. The precipitate was collected by filtration and washed with cold Et_2O to give **7c** (35 mg, 73%) as colorless solid. HPLC (UV) > 95%. mp 137–139 °C. ^{1}H NMR (400 MHz, DMSO-d_6) δ 1.23–1.37 (m, 20H), 1.61–1.64 (m, 2H), 1.83–1.91 (m, 2H), 2.20 (s, 3H, Ors-C$\underline{H}_3$), 2.60 (s, 3H, Pyr-C$\underline{H}_3$), 4.18 (t, *J* = 6.5 Hz, 2H), 4.50 (t, *J* = 7.4 Hz, 2H), 6.43 (s, 1H), 7.97 (d, *J* = 6.3 Hz, 2H), 8.91 (d, *J* = 6.7 Hz, 2H), 9.99 (s, 1H), 10.35 (s, 1H). ^{13}C NMR (100 MHz, DMSO-d_6) δ 167.8, 158.8, 154.9, 154.7, 143.7, 134.7, 128.4, 113.9, 111.3, 101.3, 64.7, 60.0, 48.7, 30.9, 29.01, 28.95, 28.92, 28.8, 28.6, 28.4, 28.1, 25.45, 25.41, 21.4, 17.5. ESI-HMRS: *m*/*z*: 490.2730 [M]$^+$ ($C_{28}H_{41}ClNO_4$ requires 490.2724).

(E)-1-(14-((2,4-dihydroxy-6-methylbenzoyl)oxy)tetradecyl)-4-(2-(8-hydroxy-2,3,6,7-tetrahydro−1*H*,5*H*-pyrido[3,2,1-ij]quinolin-9-yl)vinyl)pyridin-1-ium bromide (1a). Under inert atmosphere, 7a (340 mg, 0.63 mmol) and 9-formyl-8-hydroxyjulolidine (165 mg, 0.76 mmol) were dissolved in absolute EtOH (5.0 mL). Thereafter, piperidine (43.0 μL, 0.44 mmol) was added and the reaction mixture was stirred at 70 °C for 24 h. After cooling down to room temperature the solvent was removed under high-vacuum. The crude solid was purified by flash chromatography column on silica gel (stepwise gradient from 0 to 50% MeOH in EtOAc) leading to 1a (95 mg, 31%) as dark red solid (NOTE: the product gives a visible reddish spot in TLC that vanishes with time upon exposure to sunlight). HPLC (UV) > 92%. mp 198–202 °C. ^{1}H NMR (300 MHz, Methanol-d_4) δ 1.23–1.54 (m, 24H), 1.62–1.84 (m, 4H), 2.46 (s, 3H), 2.64 (t, *J* = 6.5 Hz, 2H), 2.70 (t, *J* = 6.3 Hz, 2H), 3.21–3.29 (m, 4H), 4.20–4.43 (m, 4H), 6.10–6.31 (m, 2H), 6.98 (d, *J* = 15.7 Hz, 1H), 7.19 (s, 1H), 7.78 (d, *J* = 6.6 Hz, 2H), 8.17 (d, *J* = 15.7 Hz, 1H), 8.39 (d, *J* = 6.6 Hz, 2H). ^{13}C NMR (126 MHz, acetic acid-d_4) δ 173.5, 166.8, 163.4, 156.8, 155.3, 148.7, 145.2, 144.1, 139.9, 127.3, 123.3, 117.2, 113.1, 112.8, 108.9, 106.4, 102.6, 66.9, 61.5, 51.6, 50.8, 32.6, 31.2, 31.1, 31.0,

30.93, 30.89, 30.6, 30.5, 30.0, 28.8, 27.6 (2C), 25.3, 23.3, 22.4. ESI-HMRS: *m/z* 655.4117 $[M]^+$ ($C_{41}H_{55}N_2O_5$ requires: 655.4111).

Ethyl 4-((14-bromotetradecyl)oxy)-2-hydroxy-6-methylbenzoate (8). Under inert atmosphere, ethyl 2,4-dihydroxy-6-methylbenzoate (300 mg, 1.53 mmol), bromotetradecan-1-ol (373 mg, 1.27 mmol), and PPh_3 (401 mg, 1.53 mmol) were dissolved in anhydrous THF (26 mL) and the flask was cooled with an ice-bath. DIAD (0.3 mL, 1.53 mmol) was added to the solution, the ice-batch was removed and the reaction mixture was kept under stirring for 2.5 h at room temperature. The organic solvent was removed under vacuum and the crude oil was washed with HCl (0.1 N, 35 mL) and extracted with AcOEt (2 × 75 mL). The combined organic layers were successively washed with water (2 × 100 mL) and brine (2 × 100 mL). The solvent was dried over $MgSO_4$, filtered and evaporated. The crude solid was purified by flash column chromatography (SiO_2; gradient from 0 to 5% EtOAc in hexanes) to give **8** as a colorless solid (395 mg, 55%). Spectroscopic data agreed with the reported ones [9].

1-(14-(4-(ethoxycarbonyl)-3-hydroxy-5-methylphenoxy)tetradecyl)-4-methylpyridin-1-ium bromide (9). Under inert atmosphere, **8** (100 mg, 0.21 mmol) and 4-methylpyridine (25 μL, 0.25 mmol) were dissolved in anhydrous CH_3CN (2 mL). The reaction was stirred at 80 °C for 3 days. After cooling down to room temperature, the solvent was removed under vacuum. The crude solid was triturated in Et_2O and the supernatant was discarded. Compound **9** was obtained as white solid (73 mg, 71%). HPLC (UV) > 95%. mp 50–54 °C. ^{1}H NMR (400 MHz, Methanol-d_4) δ 1.30–1.46 (m, 23H), 1.73–1.79 (m, 2H), 1.99–2.01 (m, 2H), 2.49 (s, 3H, Ors-C$\underline{H}_3$), 2.68 (s, 3H, Pyr-C$\underline{H}_3$), 3.97 (t, *J* = 6.4 Hz, 2H), 4.39 (q, *J* = 7.1 Hz, 2H, –COO–$\underline{CH}_2$-), 4.55 (t, *J* = 6.4 Hz, 2H), 6.28–6.31 (m, 2H), 7.93 (d, *J* = 6.3 Hz, 2H), 8.80 (d, *J* = 6.7 Hz, 2H). ^{13}C NMR (100 MHz, Methanol-d_4) δ 172.9, 166.1, 164.8, 161.3, 144.8, 144.1, 129.9, 112.0, 106.7, 100.3, 69.1, 62.3, 32.4, 30.67 (2C), 30.62, 30.58, 30.5, 30.4, 30.2, 30.1, 27.2, 27.0, 24.4, 22.0, 14.6. ESI-HMRS: *m/z*: 484.3432 $[M]^+$ ($C_{30}H_{46}NO_4$ requires 484.3427).

1-(14-(4-carboxy-3-hydroxy-5-methylphenoxy)tetradecyl)-4-methylpyridin-1-ium bromide (10). A solution of ethyl ester **9** (250 mg, 0.44 mmol) and KOH (198 mg, 3.5 mmol) in a 2:1 mixture of H_2O/MeOH (3 mL) was stirred at 50 °C for 2 days. The reaction was neutralized with aq. HCl and the solvents were evaporated to dryness. Silica chromatography of the crude solid with stepwise gradient from 0 to 50% MeOH (+few drops of AcOH) in EtOAc yielded **10** as brownish solid (170 mg, 72%). HPLC (UV) > 95%. ^{1}H NMR (400 MHz, DMSO-d_6) δ 1.09–1.42 (m, 20H), 1.64 (p, *J* = 6.7 Hz, 2H), 1.82–1.93 (m, 2H), 2.46 (s, 3H), 2.60 (s, 3H), 3.84 (t, *J* = 6.4 Hz, 2H), 4.51 (t, *J* = 7.4 Hz, 2H), 5.91 (dd, *J* = 25.2, 2.6 Hz, 2H), 7.98 (d, *J* = 6.3 Hz, 2H), 8.95 (d, *J* = 6.3 Hz, 2H). ^{13}C NMR (101 MHz, DMSO-d_6) δ 172.2, 167.0, 161.4, 159.6, 158.7, 143.7, 142.0, 128.3, 106.5, 98.8, 66.6, 59.9, 40.2, 30.6, 28.9, 28.8, 28.7, 28.6, 28.3, 25.42, 25.36, 23.44, 23.39, 21.4. ESI-LRMS: *m/z* 456 [M^+, 100%].

(E)-1-(14-(4-(ethoxycarbonyl)-3-hydroxy-5-methylphenoxy) tetradecyl)-4-(2-(8-hydroxy-2,3,6,7-tetrahydro-1H,5H-pyrido [3,2,1-ij]quinolin-9-yl)vinyl)pyridin-1-ium bromide (2a). Under inert atmosphere, 9 (1.4 g, 2.4 mmol) and 9-formyl-8-hydroxyjulolidine (592 mg, 2.73 mmol) were dissolved in absolute EtOH (5.0 mL) and piperidine (175 μL, 1.78 mmol) was added to the mixture. The reaction was heated up at 80 °C and kept under stirring for 24 h. After cooling down to room temperature the solvent was removed under high-vacuum. The crude solid was purified by flash chromatography column on silica gel (stepwise gradient from 0 to 50% MeOH in EtOAc) to give 2a (405 mg, 21%) as a reddish solid. HPLC (UV) > 95%. mr 178–198 °C. ^{1}H NMR (400 MHz, Methanol-d_4) δ 1.29–1.46 (m, 20H), 1.71–1.79 (m, 2H), 1.90–1.99 (m, 6H), 2.48 (s, 3H), 2.65 (t, *J* = 6.4 Hz, 2H), 2.70 (t, *J* = 6.5 Hz, 2H), 3.23–3.30 (m, 4H-*partially masked*), 3.94 (t, *J* = 6.4 Hz, 2H), 4.35–4.42 (m, 4H), 6.29 (d, *J* = 6.6 Hz, 2H), 6.99 (d, *J* = 15.8 Hz, 1H), 7.20 (s, 1H), 7.80 (d, *J* = 6.7 Hz, 2H), 8.17 (d, *J* = 15.8 Hz, 1H), 8.43 (d, *J* = 6.5 Hz, 2H). ^{13}C NMR (101 MHz, Methanol-d_4) δ 181.6, 172.9, 166.0, 164.8, 156.8, 155.6, 144.1, 143.8, 143.6, 140.2, 127.0, 122.6, 120.8, 116.57, 115.5, 112. 8, 112.0, 108.3, 106.7, 100.3, 69.1, 62.3, 51.2, 50.5, 32.1, 30.6, 30.5, 30.40, 30.35, 30.31, 30.1, 30.0, 28.5, 28.3, 27.0, 24.4, 23.76, 23.1, 22.9, 22.27, 22.24, 19.2, 14.6. ESI-HMRS: *m/z* 683.4419 $[M]^+$ ($C_{43}H_{59}N_2O_5$ requires 683.4424).

(E)-4-(2-(8-hydroxy-2,3,6,7-tetrahydro-1H,5H-pyrido[3,2,1-ij]quinolin-9-yl)vinyl)-1-(14-(3-hydroxy-5-methylphenoxy)tetradecyl)pyridin-1-ium bromine (2c). Compound **2c** was the sole product isolated from the reaction of **10** and 9-formyl-8-hydroxyjulolidine when following the same protocol described for the synthesis of **2a**. Purple solid (30 mg, 19%). HPLC (UV) > 95%. mp 158–162 °C. ^{1}H NMR (400 MHz, Methanol-d_4) δ 1.49–1.23 (m, 22H), 1.76–1.64 (m, 2H), 1.97–1.90 (m, 4H), 2.21 (s, 3H), 2.70–2.63 (m, 4H), 3.27–3.23 (m, 4H), 3.86 (t, *J* = 6.4 Hz, 2H), 4.34 (t, *J* = 7.3 Hz, 2H), 4.58 (bs, 1H), 6.13 (s, 1H), 6.20 (m, 2H), 6.97 (d, *J* = 15.8 Hz, 1H), 7.19 (s, 1H), 7.78 (d, *J* = 6.6 Hz, 2H), 8.18 (d, *J* = 15.8 Hz, 1H), 8.40 (d, *J* = 6.7 Hz, 2H). ^{13}C NMR (126 MHz, Methanol-d_4) δ 181.5, 161.7, 159.3, 156.9, 155.8, 148.6, 143.6, 141.1, 140.3, 132.4, 127.0, 122.5, 116.6, 115.4, 112.8, 109.5, 108.4, 107.7, 100.0, 68.8, 60.7, 30.8, 30.7, 30.6, 30.5, 30.4, 30.34, 30.28, 30.1, 30.0, 28.5, 27.14, 27.05, 23.9, 23.1, 22.3, 22.2, 21.7. ESI-HMRS: *m/z* 611.4215 $[M]^+$ ($C_{40}H_{55}N_2O_3$ requires 611.4213).

(E)-4-(2-(8-hydroxy-2,3,6,7-tetrahydro-1H,5H-pyrido[3,2,1-ij] quinolin-9-yl)vinyl)-1-(14-(3-hydroxy-4-(methoxycarbonyl)-5-methylphenoxy)tetradecyl)pyridin-1-ium bromide (2d). Secondary product from the saponification of 2a in MeOH/H_2O using KOH. To a solution of 2a (70 mg, 0.092 mmol) dissolved in methanol (1 mL) was added a solution of potassium hydroxide (102 mg, 1.8 mmol) in water (2 mL). The blueish reaction mixture was heated at 50 °C for 24 h to give a mixture of 2b and 2d as observed by HPLC–MS. The mixture was acidified with 1 M aqueous HCl solution until pH ≈ 4. The precipitate was washed with water and the crude product was purified by semi-preparative HPLC–MS. Compound 2b was not isolated pure whereas 2d was obtained as pure purple solid. HPLC (UV) > 95%. mr 80–100 °C (dec.). ^{1}H NMR (400 MHz, Methanol-d_4) δ 1.29–1.47 (m, 24H), 1.71–1.76 (m, 2H), 1.90–1.97 (m, 6H), 2.47 (s, 3H), 2.64 (t, *J* = 6.5 Hz, 2H), 2.70 (t, *J* = 6.3 Hz, 2H), 3.23–3.30 (m, 4H-*partially masked*), 3.90 (s, 3H), 3.94 (t, *J* = 6.4 Hz, 2H), 4.33 (t, *J* = 7.3 Hz, 2H), 6.28 (d, *J* = 2.6 Hz, 1H), 6.30 (d, *J* = 2.6 Hz, 1H), 6.98 (d, *J* = 15.7 Hz, 1H), 7.19 (s, 1H), 7.78 (d, *J* = 6.7 Hz, 2H), 8.17 (d, *J* = 15.8 Hz, 1H), 8.39 (d, *J* = 6.7 Hz, 2H). ESI-HMRS: *m/z* 669.4264 $[M]^+$ ($C_{42}H_{57}N_2O_5$ requires 669.4268).

1-(14-bromotetradecyl)-4-methylpyridin-1-ium (11). Under inert atmosphere, 4-methylpyridine (0.34 mL, 3.5 mmol) and 1,14-dibromotetradecane (3.0 g, 8.4 mmol) were dissolved in 10 mL of anhydrous CH_3CN. The reaction was stirred at 80 °C for 72 h. Thereafter, the mixture was allowed to cool down at 0 °C. The white precipitate obtained, was triturated with Et_2O (50 mL) and filtered over a sintered funnel. The crude solid was purified by flash chromatography column on silica gel (stepwise gradient from 0 to 50% MeOH in EtOAc) to give compound **12** as a white solid (1.0 g, 64%). mp 89–91 °C. ^{1}H NMR (400 MHz, DMSO-d_6) δ 1.20–1.37 (m, 20H), 1.65–1.69 (m, 2H), 1.83–1.91 (m, 2H), 2.30 (s, 3H), 2.61 (d, *J* = 4.0 Hz, 3H, Pyr-C$\underline{H}_3$), 3.49–3.54 (m, 2H), 4.52–4.57 (m, 2H), 7.98–8.01 (m, 2H), 8.96–8.99 (m, 2H), 10.00 (s, 1H), 10.86 (s, 1H). ^{13}C NMR (100 MHz, DMSO-d_6) δ 158.7 (-$\underline{C}$-CH_3), 143.7 (N^+-$\underline{C}$H), 128.3 (N^+-CH-$\underline{C}$H-), 59.8 (Pyr-$\underline{C}H_2$-), 35.2 (Br–$\underline{C}H_2$-), 32.2 (Br–CH_2–$\underline{C}H_2$-), 30.6 (Pyr–CH_2–$\underline{C}H_2$-), 29.0, 28.9, 28.9, 28.8, 28.4, 28.1, 27.5, 25.4, 21.4 (Pyr-$\underline{C}H_3$). ESI-HMRS: *m/z* 368.1955 [M]+($C_{20}H_{35}BrN$ requires 368.1953).

(E)-1-(14-bromotetradecyl)-4-(2-(8-hydroxy-2,3,6,7-

tetrahydro-1H,5H-pyrido[3,2,1-ij]quinolin-9-yl)vinyl)pyridin-1-ium (12). Under inert atmosphere, compound **11** (530 mg, 1.18 mmol) and 9-formyl-8-hydroxyjulolidine (283 mg, 1.3 mmol) were dissolved in 6.0 mL of EtOH. Then, piperidine (58 μL, 0.59 mmol) was added to the solution. The reaction was stirred at 80 °C for 1.5 h. After cooling down at room temperature, the solvent was removed under high vacuum. The crude solid was purified by flash chromatography column on silica gel (stepwise gradient from 0 to 10% MeOH in EtOAc) to yield **12** as a red-like solid (30 mg, 7%). mp > 120 °C (dec.). ^{1}H NMR (400 MHz, $CDCl_3$) δ 1.20–1.37 (m, 20H), 1.56–1.69 (m, 2H), 1.78–1.89 (m, 2H), 1.91–1.98 (m, 4H), 2.67 (t, J = 6.3 Hz, 2H), 2.81 (t, J = 6.3 Hz, 2H), 3.20–3.27 (m, 4H), 3.40 (t, J = 6.9 Hz, 2H, Pyr-C$\underline{H}_2$-), 4.25 (t, J = 7.4 Hz, 2H, Br–C$\underline{H}_2$-), 6.56 (d, J = 15.4 Hz, 1H), 7.04 (s, 1H), 7.84 (d, J = 6.5 Hz, 2H), 8.11 (bs, 1H, OH), 8.21 (d, J = 6.6 Hz, 2H), 8.40 (d, J = 15.4 Hz, 1H). ^{13}C NMR (100 MHz, $CDCl_3$) δ 155.3, 155.1, 147.9, 141.5, 140.6, 125.0, 122.2, 115.4, 113.5, 111.0, 107.8, 59.9, 50.4, 49.9, 34.3, 33.0, 31.4, 29.7, 29.7, 29.6, 29.6, 29.5, 29.2, 29.0, 28.9, 28.3, 27.6, 26.3, 22.1, 21.7, 21.2. ESI-HMRS: m/z 567.2956 $[M]^+$ ($C_{33}H_{48}BrN_2O$ requires 567.2950).

4.3. Photophysical characterization

Absorption spectra were recorded employing a Lambda 650 double-beam UV spectrophotometer (PerkinElmer, USA), steady-state fluorescence emission were recorded by an FP-8500 spectrofluorimeter (Jasco, Japan), and fluorescence lifetimes were obtained by collecting five fluorescence decay traces, between 570 and 650 nm (Δλ = 20 nm), using a FluoTime 200 time-resolved fluorometer (PicoQuant, Germany) employing a 530-nm pulsed diode laser (LDH-530, PicoQuant, Germany) with a repetition rate of 20 MHz. Average fluorescence lifetimes, τ_{av}, were obtained by global fitting the decay traces to tri-exponential decay functions, and using the equation

$$\tau_{av} = \frac{\sum_i p_i \cdot \tau_i}{\sum_i p_i}$$

Where τ_i are the individual fluorescence decay times and p_i are the corresponding preexponential factors, to estimate the average at each emission wavelength. We then obtained the average of the τ_{av} values for only the wavelengths in which all the preexponential factors were positive.

Quantum yield values were estimated measured using the relative method and rhodamine 101 in methanol (ϕ = 1) as the reference standard [46].

4.4. Ab initio calculations

All molecular orbital calculations were performed using the Gaussian 09 quantum chemical package. Ground state geometry of the molecule **1a** was optimized using the DFT hybrid functional, B3LYP [47,48]. Pople's basis set with both diffuse and polarization functions, 6-31 + G** was used for all the atoms. The compound of interest **1a** was subjected of geometry optimization in the i) ground state using B3LYP/6-31 + G** level of theory and ii) excited state using time dependent density functional theory (TD-DFT) with similar hybrid functional. Both optimizations used the same IEFPCM solvation in EtOH.

4.5. Biology

4.5.1. Drug sensitivity assay in bloodstream forms T. b. brucei

The resazurin (Alamar blue) assay [49] was used to determine the susceptibilities of bloodstream trypomastigotes of *T. b. brucei*: wild-type (s427 WT), and the drug resistant strains B48 and AQP1-3 KO; B48 is derived from s427 WT by subsequently deleting the *TbAT1* drug transporter gene [50] and in vitro adaptation to high concentrations of pentamidine [24], whereas AQP1-3 KO is a strain from which all aquaporin genes were deleted [25], including the pentamidine- and arsenicals-transporting TbAQP2 [28]. Cells were grown at 37 °C in a 5% CO_2 atmosphere in Hirumi's Modifed Iscove's medium 9 (HMI-9; Life Technologies) supplemented with 10% (*vol/vol*) heat-inactivated Fetal Calf Serum (FCS; Biosera), 3.0 g/L sodium hydrogen carbonate (Sigma) per litre of medium, and 14 μL/L β-mercaptoethanol (Sigma), pH 7.4 (complete HMI-9).

A double dilution of the test compounds was prepared in 100 μL of the same medium over 2 rows (23 wells), with the 24th well receiving 100 μL of medium as drug-free control. The cell density was adjusted to 2×10^5 cells/mL in complete HMI-9 after which 100 μL of this suspension was added to each well of the 96-well plate containing the serially diluted test compounds.

The plate containing trypanosomes and test compound was incubated at 37 °C in a 5% CO_2 atmosphere for a period of 48 h, followed by the addition of 20 μL of a 500 μM filter-sterilised resazurin sodium salt (Sigma) solution in PBS (pH 7.4), and a further 24-h incubation. The standard trypanocide pentamidine (Sigma) was used as positive control. Fluorescence was measured in a FLUOstar Optima plate reader (BMG Labtech, Durham, NC, USA) at wavelengths of 544 nm for excitation, 590 for emission. EC_{50} values were determined by non-linear regression using an equation for a sigmoidal dose-response curve with variable slope (GraphPad Prism 7.0, GraphPad Software Inc., San Diego, CA, USA). The EC_{50} values were obtained from at least 3 independent experiments.

4.5.2. Cell culture and cytotoxicity of the test compounds on human embryonic kidney cells

The inhibitors were tested for their toxicity on Human Embryonic Kidney (HEK) cells (strain 293T), essentially as described previously [51]. HEK cells were grown as a monolayer in a standard filtered-sterile culture that comprised 500 mL Dulbecco's Modified Eagle's Medium (DMEM; Sigma), glutamine (0.58 g/L), and 10 mL/L of 100 × penicillin and streptomycin (PenStrep; Thermo Fisher Scientific, Waltham, MA, USA), supplemented with 50 mL heat-inactivated foetal bovine serum (Thermo Fisher Scientific). The cells were cultured and incubated at 37 °C under a humidified 5% CO_2 atmosphere, and were passaged when reaching 80–85% confluence in a vented flask.

For the toxicity assay, cells were adjusted to the desired density of 3×10^5 cells/mL, of which 100 μL was added to each well of a 96-well plate. To allow cell adhesion, the plate was incubated for 24 h. Serial drug dilutions of the test compounds (130 μL) were made in a separate 96-well sterile plate. Using a multichannel pipette, 100 μL of these dilutions (test compounds) were transferred to the corresponding wells of the 96-well sterile plate containing the cells, with the last well receiving 100 μL of medium as drug-free control. Phenylarsine oxide (PAO) was used as positive control. The plate containing the cells and test compounds was then incubated for an additional 30 h at 37 °C/5% CO_2. After this, 10 μL of resazurin solution (125 mg/L in PBS) was added to every well of the plate before a final 24-h incubation (37 °C/5% CO_2). The plate was read in a FLUOstar OPTIMA fluorimeter at wavelengths 530 nm for excitation and 590 nm for emission. Analysis of the data to determine the EC_{50} values was done using GraphPad Prism 7.0.

4.5.3. Ubiquinol oxidase/TAO inhibitory assay

The Ubiquinol oxidase activity of recombinant TAO lacking the mitochondrial targeting signal (ΔMTS) was carried out exactly according to a previously published protocol for TAO inhibition assay [10]. Briefly, ΔMTS TAO activity was determined using a V-630 Jasco

UV–Vis spectrophotometer (Jasco Corporation, Tokyo, Japan) by measuring the absorbance change of the substrate-ubiquinol (ε_{278} = 15,000 M^{-1} cm^{-1}) at 278 nm over a period of 2 min in a 1 cm cuvette. The enzyme was pre-incubated for 2 min in a 50 mM Tris–HCl (pH 7.4) buffer containing the detergent octaethylene glycol monododecylether (0.05% (w/v)) in a total reaction volume of 1 mL at 25 °C. Reactions were initiated by the addition of ubiquinol to the cuvette.

The inhibition reaction was carried out by pre-incubating a fixed amount of rTAO with varying amounts of the inhibitor for 2 min in the same buffer before adding the substrate. DMSO and Ascofuranone/SHAM were used as negative and positive controls, respectively. Control experiments were also carried out throughout the experiment to verify that there was no auto-oxidation of ubiquinol in the medium. Residual activities were plotted against the corresponding inhibitor concentration to generate the IC_{50} using GraphPad Prism.

4.5.4. Real-time measurement of fluorescence in T. b. brucei

Cultures of *T. b. brucei* bloodstream forms in mid-log growth phase of either 427WT or *aqp1-3 null* strains were centrifuged for 10 min at 800×*g*, washed twice in assay buffer by centrifugation at 2400 rpm and resuspended at a density of 10^8 cells/mL and the cell suspension was distributed into wells of a 96-well plate (200 μL/well). The plate was transferred to a microplate reader (FLUOstar Optima, BMG Labtech) equipped with atmospheric controls set at 37 °C and 5% CO_2, and fluorescence read using 544/620 excitation and emission filters. After a pre-set time to record background fluorescence, the reading was paused and 20 μL of compound **2a** or **12** was added into respective wells to a final concentration of 0.2 μM or 2 μM as indicated, followed by continuation of the reading. For some experiments the measurement was paused again at 80 min and 20 μL of either PBS pH7.4, TAO47, TAO38 (to final concentration of 0.2 μM) or 100 mM glycerol (10 mM final concentration) was added to respective wells and reading continued.

4.5.5. Mitochondrial staining in T. brucei

1 mL *T. b. brucei* cells prepared at a density of 2 × 10^6 cells/mL were incubated with 4 μM, 8 μM and 40 μM of compound **1a** in complete HMI-9 for 1 h (37 °C, 5% CO_2). MitoTracker™ Green FM (Invitrogen, M7514) was added to the cells to a final concentration of 100 nM, followed by further incubation for 10 min. The cells were then centrifuged at 1000×*g* for 10 min, and the pellet was washed once in 1 mL of 1 × sterile PBS pH 7.4, and resuspended in 50 μL PBS. The sample was then prepared and incubated in 5 mg/mL of Hoechst 33342 Staining Dye Solution (Abcam, ab228551) in the dark at room temperature for 10 min. This was followed by another wash in 1 mL of 1 × cold sterile PBS and the cells were resuspended in 20 mL of ice-chilled PBS-primed CyGEL™ (Abcam, ab109204) in order to gently immobilise the trypanosomes. The mixture was transferred into a clean slide on ice, covered with coverslip and sealed with nail varnish**.** Images were obtained immediately under DeltaVision microscope (GE Healthcare) using softWoRx software and processed using ImageJ software**.**

4.5.6. Accumulation of 1a in rat liver mitochondria

We homogenized rat liver in 20 mM HEPES (4-(2-hydroxyethyl)-1-piperazineethanesulfonic acid) 250 mM sucrose pH 7.4 buffer (1:10; m:w) using a mechanical potter. After two cycles of centrifuging at 800×*g* and washing to precipitate nuclei and undamaged cells, the supernatant was centrifuged at 9000×*g* to obtain a fraction enriched in mitochondria that were resuspended in HEPES-sucrose buffer.

The dyes were dissolved at 3 × 10^{-7} M in HEPES-sucrose buffer, pH = 7.4, and the emission spectra were measured with both 470 and 540 nm excitation. For comparison, the dyes were dissolved in the mitochondrial suspension at the same concentration and incubated for 20 min at room temperature. The suspension was then centrifuged at 10,000×*g* for 10 min and the supernatant was separated and its emission spectra were measured at the same instrumental conditions. The relative amount of partitioned dye in mitochondria was estimated by comparing the total area under the spectral curve in the supernatant and in the control solution. We report the average value of two different repeated experiments (using different mitochondrial extracts) and averaged at the different excitation wavelengths employed. Reliable results were only obtained with **1a**. For the other dyes, the quantum yield in aqueous solution was so low that made this method impractical.

4.5.7. Fluorescence microscopy in human cells

MC3T3-E1 preosteoblast (ECACC 99072810) cell line was provided by the Cell Culture Facility, University of Granada. MC3T3-E1 cells were grown in alpha minimum essential medium (αMEM) containing 10% (v/v) fetal bovine serum, 2 mM glutamine, 100 U/mL penicillin, and 0.1 μg/mL streptomycin in a humidified 5% CO_2 incubator. For microscopy experiments, MC3T3-E1 cells were seeded onto μ-Slide 8 Well Glass Bottom (Ibidi GmbH, Gräfelfing, Germany) at a density of 25,000 cells/well.

For single-photon excitation mitochondrial localization studies we employed an Abberior Expert Line Confocal Microscope (Abberior, Germany) recording data into two different channels: a first channel with a 561-nm pulsed diode laser as excitation source and a detection window of 580–630 nm and a second channel with an excitation source of 640-nm pulsed diode laser and a detection window of 650–720 nm. Data were collected employing alternating excitation for each channel to avoid crosstalk interferences. Cells were preincubated with **1a**, **2a** and **2c** 0.6 μM, respectively 30 min at 37 °C and, after that, Mitotracker Deep Red (ThermoFisher Scientific, USA) were added to obtain a final concentration of 16 nM and incubated 30 min at 37 °C before measure. Pearson's coefficients were estimated using dedicated macros on FiJi (an ImageJ distribution) [52], having reported the average value from 12 different images for **1a**, 7 images for **2a** and 5 images for **2c**. Errors in the Pearson's coefficient values are expressed as standard deviation.

Two-photon absorption fluorescence imaging was performed on a Leica TCS-SP5 II (Leica, Germany), equipped with a MaiTai Ti:Sapphire fs-pulsed tunable laser (Spectra Physics, USA). We employed excitation at 850 nm, which permitted simultaneous excitation of **1a** and Mitotracker Green (MTG), and two channels of detection, 500–550 nm for MTG and 600–650 for collecting emission of TAO inhibitors. For these experiment cells were seeded onto coverslips in 12 well-plates with a density of 9 × 10^5 cell/well and incubated at 37 °C during 24 h. Cells were preincubated with 16 nM MTG for 30 min before the addition of **1a**, and further 30 min incubation at 37 °C. Then, cells were fixed with 2% of paraformaldehyde in PBS during 15 min at room temperature.

Declaration of competing interest

The authors declare that they have no known competing financial interests or personal relationships that could have appeared to influence the work reported in this paper.

Acknowledgements

This work was supported by the Spanish Ministerio de Economia y Competitividad (grant SAF2015-66690-R), the Spanish Ministerio de Ciencia, Innovación y Universidades (MCIU/AEI/FEDER, UE; grants RTI2018-093940-B-I00 to CD, and CTQ2017-85658-R to

AO) and the Japan Society for the promotion of Science (JSPS grant-17F17420 to GUE). MAU is funded through a studentship from the Petroleum Technology Development Fund (PTDF), Abuja, Nigeria. IAA was funded through a Ph.D. studentship from the Ministry of Health of Saudi Arabia. We thank Dr. José Cumella for the synthesis of the 1,14-dibromotetradecane precursor and to Prof. Ibon Alkorta for his help with DFT calculations. We also thank Professor Fred Opperdoes and Dr Alena Zíková for their insightful discussions on *T. brucei* energy metabolism.

Appendix A. Supplementary data

Supplementary data to this article can be found online at https://doi.org/10.1016/j.ejmech.2021.113470.

References

[1] WHO fact sheet 259. http://www.who.int/mediacentre/factsheets/fs259/en/. (Accessed 29 July 2020).
[2] H.P. De Koning, The drugs of sleeping sickness: their mechanisms of action and resistance, and a brief history, Trav. Med. Infect. Dis. 5 (1) (2020) 14.
[3] F. Giordani, L.J. Morrison, T.G. Rowan, H.P. De Koning, M.P. Barrett, The animal trypanosomiases and their chemotherapy: a review, Parasitology 143 (14) (2016) 1862–1889.
[4] P.T. Grant, J.R. Sargent, Properties of L-alpha-glycerophosphate oxidase and its role in the respiration of *Trypanosoma rhodesiense*, Biochem. J. 76 (1960) 229–237.
[5] A.B. Clarkson Jr., E.J. Bienen, G. Pollakis, R.W. Grady, Respiration of bloodstream forms of the parasite *Trypanosoma brucei brucei* is dependent on a plant-like alternative oxidase, J. Biol. Chem. 264 (30) (1989) 17770–17776.
[6] S.K. Menzies, L.B. Tulloch, G.J. Florence, T.K. Smith, The trypanosome alternative oxidase: a potential drug target? Parasitology 145 (2) (2016) 175–183.
[7] T. Shiba, Y. Kido, K. Sakamoto, D.K. Inaoka, C. Tsuge, R. Tatsumi, G. Takahashi, E.O. Balogun, T. Nara, T. Aoki, T. Honma, A. Tanaka, M. Inoue, S. Matsuoka, H. Saimoto, A.L. Moore, S. Harada, K. Kita, Structure of the trypanosome cyanide-insensitive alternative oxidase, Proc. Natl. Acad. Sci. Unit. States Am. 110 (12) (2013) 4580–4585.
[8] G.U. Ebiloma, E.O. Balogun, E.J. Cueto-Díaz, H.P. de Koning, C. Dardonville, Alternative oxidase inhibitors: mitochondrion-targeting as a strategy for new drugs against pathogenic parasites and fungi, Med. Res. Rev. 39 (2019) 1553–1602.
[9] A. Meco-Navas, G.U. Ebiloma, A. Martín-Domínguez, I. Martínez-Benayas, E.J. Cueto-Díaz, A.S. Alhejely, E.O. Balogun, M. Saito, M. Matsui, N. Arai, T. Shiba, S. Harada, H.P. De Koning, C. Dardonville, SAR of 4-alkoxybenzoic acid inhibitors of the trypanosome alternative oxidase, ACS Med. Chem. Lett. 9 (9) (2018) 923–928.
[10] G.U. Ebiloma, T. Díaz Ayuga, E.O. Balogun, L. Abad Gil, A. Donachie, M. Kaiser, T. Herraiz, D.K. Inaoka, T. Shiba, S. Harada, K. Kita, H.P. de Koning, C. Dardonville, Inhibition of trypanosome alternative oxidase without its N-terminal mitochondrial targeting signal (ΔMTS-TAO) by cationic and non-cationic 4-hydroxybenzoate and 4-alkoxybenzaldehyde derivatives active against *T. brucei* and *T. congolense*, Eur. J. Med. Chem. 150 (2018) 385–402.
[11] F.J. Fueyo González, G.U. Ebiloma, C. Izquierdo García, V. Bruggeman, J.M. Sánchez Villamañán, A. Donachie, E.O. Balogun, D.K. Inaoka, T. Shiba, S. Harada, K. Kita, H.P. De Koning, C. Dardonville, Conjugates of 2,4-dihydroxybenzoate and salicylhydroxamate and lipocations display potent antiparasite effects by efficiently targeting the *Trypanosoma brucei* and *Trypanosoma congolense* mitochondrion, J. Med. Chem. 60 (4) (2017) 1509–1522.
[12] G. Zhang, Y. Sun, X. He, W. Zhang, M. Tian, R. Feng, R. Zhang, X. Li, L. Guo, X. Yu, S. Zhang, Red-emitting mitochondrial probe with ultrahigh signal-to-noise ratio enables high-fidelity fluorescent images in two-photon microscopy, Anal. Chem. 87 (24) (2015) 12088–12095.
[13] Z.R. Grabowski, K. Rotkiewicz, W. Rettig, Structural changes accompanying intramolecular electron Transfer: focus on twisted intramolecular charge-transfer states and structures, Chem. Rev. 103 (10) (2003) 3899–4032.
[14] M.A. Haidekker, E.A. Theodorakis, Environment-sensitive behavior of fluorescent molecular rotors, J. Biol. Eng. 4 (1) (2010) 11.
[15] M. Chaudhuri, R.D. Ott, G.C. Hill, Trypanosome alternative oxidase: from molecule to function, Trends Parasitol. 22 (10) (2006) 484–491.
[16] Chen R., Rubenstein A.E., Yu J.-C., Winssinger N., Barluenga S., Treatment of Neurofibromatosis with Radicicol and its Derivatives. US Patent 8,329,683 B2, 2012. http://patft.uspto.gov/netacgi/nph-Parser?Sect1=PTO1&Sect2=HITOFF&p=1&u=/netahtml/PTO/srchnum.html&r=1&f=G&l=50&d=PALL&s1=8329683.PN.
[17] E. Moulin, V. Zoete, S. Barluenga, M. Karplus, N. Winssinger, Design, synthesis, and biological evaluation of HSP90 inhibitors based on conformational analysis of radicicol and its analogues, J. Am. Chem. Soc. 127 (19) (2005) 6999–7004.
[18] N.S. Curvey, S.E. Luderer, J.K. Walker, G.W. Gokel, Improved syntheses of benzyl hydraphile synthetic cation-conducting channels, Synthesis 46 (20) (2014) 2771–2779.
[19] C. Girlanda-Junges, F. Keyling-Bilger, G. Schmitt, B. Luu, Effect of cyclohexenonic long chain fatty alcohols on neurite outgrowth. Study on structure-activity relationship, Tetrahedron 54 (27) (1998) 7735–7748.
[20] D.S. Patil, K.C. Avhad, M.M. Kadam, N. Sekar, Synthesis of red emitting triphenylamine derived NLOphoric D–π–A molecules: photophysical, and viscosity sensing studies, SN Appl. Sci. 1 (3) (2019) 259.
[21] X. Liu, W. Chi, Q. Qiao, S.V. Kokate, E.P. Cabrera, Z. Xu, X. Liu, Y.-T. Chang, Molecular mechanism of viscosity sensitivity in BODIPY rotors and application to motion-based fluorescent sensors, ACS Sens. 5 (3) (2020) 731–739.
[22] A. Vyšniauskas, M. Qurashi, N. Gallop, M. Balaz, H.L. Anderson, M.K. Kuimova, Unravelling the effect of temperature on viscosity-sensitive fluorescent molecular rotors, Chem. Sci. 6 (10) (2015) 5773–5778.
[23] S. Sasaki, G.P.C. Drummen, G.-i. Konishi, Recent advances in twisted intramolecular charge transfer (TICT) fluorescence and related phenomena in materials chemistry, J. Mater. Chem. C 4 (14) (2016) 2731–2743.
[24] D.J. Bridges, M.K. Gould, B. Nerima, P. Mäser, R.J.S. Burchmore, H.P. De Koning, Loss of the high-affinity pentamidine transporter is responsible for high levels of cross-resistance between arsenical and diamidine drugs in african trypanosomes, Mol. Pharmacol. 71 (4) (2007) 1098–1108.
[25] L. Jeacock, N. Baker, N. Wiedemar, P. Mäser, D. Horn, Aquaglyceroporin-null trypanosomes display glycerol transport defects and respiratory-inhibitor sensitivity, PLoS Pathog. 13 (3) (2017), e1006307.
[26] P.T. Grant, J.D. Fulton, The catabolism of glucose by strains of *Trypanosoma rhodesiense*, Biochem. J. 66 (2) (1957) 242–250.
[27] H.P. de Koning, S.M. Jarvis, Uptake of pentamidine in *Trypanosoma brucei brucei* is mediated by the P2 adenosine transporter and at least one novel, unrelated transporter, Acta Trop. 80 (3) (2001) 245–250.
[28] A.H. Alghamdi, J.C. Munday, G.D. Campagnaro, D. Gurvic, F. Svensson, C.E. Okpara, A. Kumar, J. Quintana, M.E. Martin Abril, P. Milic, L. Watson, D. Paape, L. Settimo, A. Dimitriou, J. Wielinska, G. Smart, L.F. Anderson, C.M. Woodley, S.P.Y. Kelly, H.M. Ibrahim, F. Hulpia, M.I. Al-Salabi, A.A. Eze, T. Sprenger, I.A. Teka, S. Gudin, S. Weyand, M. Field, C. Dardonville, R.R. Tidwell, M. Carrington, P. O'Neill, D.W. Boykin, U. Zachariae, H.P. De Koning, Positively selected modifications in the pore of TbAQP2 allow pentamidine to enter *Trypanosoma brucei*, Elife 9 (2020), e56416.
[29] R.A. West, O.G. O'Doherty, T. Askwith, J. Atack, P. Beswick, J. Laverick, M. Paradowski, L.E. Pennicott, S.P.S. Rao, G. Williams, S.E. Ward, African trypanosomiasis: synthesis & SAR enabling novel drug discovery of ubiquinol mimics for trypanosome alternative oxidase, Eur. J. Med. Chem. 141 (Supplement C) (2017) 676–689.
[30] B. Kunze, G. Hofle, H. Reichenbach, The aurachins, new quinoline antibiotics from myxobacteria: production, physico-chemical and biological properties, J. Antibiot. 40 (3) (1987) 258–265.
[31] C.A. Lanteri, R.R. Tidwell, S.R. Meshnick, The mitochondrion is a site of trypanocidal action of the aromatic diamidine DB75 in bloodstream forms of *Trypanosoma brucei*, Antimicrob. Agents Chemother. 52 (3) (2008) 875–882.
[32] H.M.S. Ibrahim, M.I. Al-Salabi, N.E. Sabbagh, N.B. Quashie, A.A.M. Alkhaldi, R. Escale, T.K. Smith, H.J. Vial, H.P. De Koning, Symmetrical choline-derived dications display strong anti-kinetoplastid activity, J. Antimicrob. Chemother. 66 (1) (2011) 111–125.
[33] A.A. Eze, M.K. Gould, J.C. Munday, D.N. Tagoe, V. Stelmanis, A. Schnaufer, H.P. De Koning, Reduced mitochondrial membrane potential is a late adaptation of *Trypanosoma brucei brucei* to isometamidium preceded by mutations in the gamma subunit of the F1Fo-ATPase, PLoS Neglected Trop. Dis. 10 (8) (2016), e0004791.
[34] C. Dardonville, A.A.M. Alkhaldi, H.P. De Koning, SAR studies of diphenyl cationic trypanocides: superior activity of phosphonium over ammonium salts, ACS Med. Chem. Lett. 6 (2) (2015) 151–155.
[35] A. Taladriz, A. Healy, E.J. Flores Pérez, V. Herrero García, C. Ríos Martínez, A.A.M. Alkhaldi, A.A. Eze, M. Kaiser, H.P. De Koning, A. Chana, C. Dardonville, Synthesis and structure-activity analysis of new phosphonium salts with potent activity against African trypanosomes, J. Med. Chem. 55 (6) (2012) 2606–2622.
[36] A.A.M. Alkhaldi, J. Martinek, B. Panicucci, C. Dardonville, A. Zíková, H.P. de Koning, Trypanocidal action of bisphosphonium salts through a mitochondrial target in bloodstream form *Trypanosoma brucei*, Int. J. Parasitol. Drugs Drug Resist. 6 (1) (2016) 23–34.
[37] D.J. Hammond, I.B.R. Bowman, Studies on glycerol kinase and its role in ATP synthesis in *Trypanosoma brucei*, Mol. Biochem. Parasitol. 2 (2) (1980) 77–91.
[38] F.R. Opperdoes, P. Borst, Localization of nine glycolytic enzymes in a microbody-like organelle in *Trypanosoma brucei*: the glycosome, FEBS Lett. 80 (2) (1977) 360–364.
[39] B. Bassarak, N.L. Uzcátegui, C. Schönfeld, M. Duszenko, Functional characterization of three aquaglyceroporins from *Trypanosoma brucei* in osmoregulation and glycerol transport, Cell. Physiol. Biochem. 27 (3–4) (2011) 411–420.
[40] M. Serricchio, P. Bütikofer, Phosphatidylglycerophosphate synthase associates with a mitochondrial inner membrane complex and is essential for growth of *Trypanosoma brucei*, Mol. Microbiol. 87 (3) (2013) 569–579.
[41] M. Serricchio, P. Bütikofer, An essential bacterial-type cardiolipin synthase mediates cardiolipin formation in a eukaryote, Proc. Natl. Acad. Sci. Unit. States Am. 109 (16) (2012) E954.
[42] M. Serricchio, C. Hierro-Yap, D. Schädeli, H. Ben Hamidane, A. Hemphill, J. Graumann, A. Zíková, P. Bütikofer, Depletion of cardiolipin induces major changes in energy metabolism in *Trypanosoma brucei* bloodstream forms,

FASEB J. 35 (2021) e21176.
[43] F. Castello, J.M. Paredes, M.J. Ruedas-Rama, M. Martin, M. Roldan, S. Casares, A. Orte, Two-step amyloid aggregation: sequential lag phase intermediates, Sci. Rep. 7 (1) (2017) 40065.
[44] P. Herrero-Foncubierta, M.d.C. González-García, S. Resa, J.M. Paredes, C. Ripoll, M.D. Girón, R. Salto, J.M. Cuerva, A. Orte, D. Miguel, Simple and non-charged long-lived fluorescent intracellular organelle trackers, Dyes Pigments 183 (2020), 108649.
[45] P. Wang, Z. Zhang, B. Yu, Total synthesis of CRM646-A and -B, two fungal glucuronides with potent heparinase inhibition activities, J. Org. Chem. 70 (22) (2005) 8884–8889.
[46] A.M. Brouwer, Standards for photoluminescence quantum yield measurements in solution (IUPAC Technical Report), Pure Appl. Chem. 83 (12) (2011) 2213–2228.
[47] M. Ravi, A. Samanta, T.P. Radhakrishnan, Excited state dipole moments from an efficient analysis of solvatochromic Stokes shift data, J. Phys. Chem. 98 (37) (1994) 9133–9136.
[48] E.G. McRae, Theory of solvent effects on molecular electronic spectra. Frequency shifts, J. Phys. Chem. B 61 (5) (1957) 562–572.
[49] M.K. Gould, X.L. Vu, T. Seebeck, H.P. de Koning, Propidium iodide-based methods for monitoring drug action in the kinetoplastidae: comparison with the Alamar Blue assay, Anal. Biochem. 382 (2) (2008) 87–93.
[50] E. Matovu, M.L. Stewart, F. Geiser, R. Brun, P. Mäser, L.J.M. Wallace, R.J. Burchmore, J.C.K. Enyaru, M.P. Barrett, R. Kaminsky, T. Seebeck, H.P. De Koning, Mechanisms of arsenical and diamidine uptake and resistance in *Trypanosoma brucei*, Eukaryot. Cell 2 (5) (2003) 1003–1008.
[51] B. Rodenko, M.J. Wanner, A.A.M. Alkhaldi, G.U. Ebiloma, R.L. Barnes, M. Kaiser, R. Brun, R. McCulloch, G.-J. Koomen, H.P. de Koning, Targeting the parasite's DNA with methyltriazenyl purine analogs is a safe, selective, and efficacious antitrypanosomal strategy, Antimicrob. Agents Chemother. 59 (11) (2015) 6708–6716.
[52] J. Schindelin, I. Arganda-Carreras, E. Frise, V. Kaynig, M. Longair, T. Pietzsch, S. Preibisch, C. Rueden, S. Saalfeld, B. Schmid, J.-Y. Tinevez, D.J. White, V. Hartenstein, K. Eliceiri, P. Tomancak, A. Cardona, Fiji: an open-source platform for biological-image analysis, Nat. Methods 9 (7) (2012) 676–682.